Marine Pollution Bulletin 234 (2027) 120464

Contents lists available at ScienceDirect

Marine Pollution Bulletin

journal homepage: www.elsevier.com/locate/marpolbul

Polystyrene microplastic induced immunotoxicity and redox dysregulation in the tropical sand star *Astropecten euryacanthus* of the Bay of Bengal: An integrated biomarker approach

Abhinandan Barua [a], Nairit Panday [a], Ritwik Guchait [b], Pritam Sinha [c], Arunodaya Gautam [a,*], Indrani Chakraborty [d,*]

[a] *Estuarine and Coastal Studies Foundation, Howrah, West Bengal, 711101, India*
[b] *Maulana Abul Kalam Azad University of Technology, Bidhannagar, Kolkata, West Bengal, 700064, India*
[c] *Department of Physical Science, BOSE INSTITUTE UNIFIED ACADEMIC CAMPUS, EN 80, Bidhannagar, EN Block, Sector V, Kolkata, Bidhannagar, West Bengal, 700091, India*
[d] *Jogamaya Devi College, 92, S.P. Mukherjee Road, Kolkata, West Bengal, 700026, India*

ARTICLE INFO

Keywords:
Polystyrene microplastics
Sand star
Coelomocytes
Reactive oxygen species
Antioxidation
Integrated biomarker response

ABSTRACT

Polystyrene microplastics (PS-MPs) are emerging contaminants increasingly detected in coastal ecosystems, but quantitative information on PS-MP-associated immunotoxicity in tropical benthic asteroids of the Bay of Bengal remains limited. This study hypothesised that exposure to experimental PS-MP concentrations, which exceed typical environmental concentrations, would disrupt immune regulation and redox homeostasis in the tropical sea star *Astropecten euryacanthus*.

Adult specimens were exposed to PS-MPs (0.25, 0.5, and 1 mg/L) for 7 and 14 days under controlled laboratory conditions to assess immunophysiological and oxidative stress responses. PS-MP exposure increased total coelomocyte abundance, indicating an activated cellular immune response. Flow cytometry revealed a reduction in G1-gated blast-like cells from 8.87% to 2.84% and an increase in G3-gated petaloid cells from 8.88% to 20.15% at 1 mg/L, indicating marked changes in coelomocyte population distribution. Oxidative imbalance was evident from increased superoxide anion production and intracellular reactive oxygen species, particularly in G1-gated coelomocytes. Superoxide dismutase and catalase activities declined, whereas glutathione-S-transferase activity increased, suggesting differential regulation of antioxidant and detoxification pathways. The integrated biomarker response (IBR/n) provided a descriptive representation of the combined biomarker responses and demonstrated concentration- and exposure-duration-dependent variation in the overall biomarker profile. Future studies should evaluate chronic responses to lower, environmentally relevant PS-MP concentrations, particularly because the concentrations examined in the present study represent acute dose exposure scenarios relative to field concentrations.

Collectively, These findings suggest the biomonitoring potential of *A. euryacanthus* for evaluating microplastic-associated environmental risks in tropical benthic habitats of coastal ecosystem.

1. Introduction

Microplastics (MPs) are processed or fragmented polymers with a size range below 5 mm. are classified into primary and secondary MPs based on their source and weathering process (Chatterjee et al., 2025). The environmental fate and transport of MPs are governed by their physicochemical properties, hydrodynamic conditions, and interactions with biological and chemical components, which can promote their redistribution and accumulation in water columns and sediments (Shiry et al., 2026). Sediment-associated MPs may increase the exposure potential of benthic organisms, including *A. euryacanthus*, which closely interact with contaminated substrates. The ingestion of MPs by planktonic, benthic, and pelagic organisms poses a serious immunophysiological threat to these organisms (Tang et al., 2018). Marine MPs, which

* Corresponding authors.
E-mail addresses: baruaabhinandan@gmail.com (A. Barua), nairitpanday57@gmail.com (N. Panday), rguchait57@gmail.com (R. Guchait), pritam.sinha@jcbose.ac.in (P. Sinha), arunodayagautam@ecsfindia.org (A. Gautam), indrani.nrs@gmail.com (I. Chakraborty).

https://doi.org/10.1016/j.marpolbul.2026.120464
Received 15 July 2026; Received in revised form 8 October 2026; Accepted 9 October 2026
Available online 14 October 2026
0025-326X/© 2026 Elsevier Ltd. All rights are reserved, including those for text and data mining, AI training, and similar technologies.

are complex cocktail polymers, residual monomers, and chemical additives, can induce cellular and molecular toxicity in consumer organisms (Teuten et al., 2009). Despite the increasing evidence of microplastic toxicity, the immunological effects of microplastic exposure in echinoderms remain poorly characterised. Polystyrene is a synthetic aromatic polymer derived from styrene, which has been identified as a substance of toxicological concern and possesses genotoxic potential (EFSA Panel on Food Contact Materials, Enzymes and Processing Aids, 2020). Polystyrene microplastics (PS-MPs) have been documented as a major MPs in the coastal water and sediments of the Bay of Bengal (Alam et al., 2023). This study investigated the immunophysiological responses of *A. euryacanthus* to PS-MP exposure and evaluated coelomocyte-based biomarkers as a novel tool for biomonitoring MP pollution in the Bay of Bengal. This study addresses a critical knowledge gap regarding PS-MP-induced immunotoxicity in tropical asteroids and provides an integrated biomarker-based framework for assessing the ecotoxicological effects of these microplastics.

Echinoderms are considered suitable bioindicators of marine pollution because of their ecological importance, wide distribution, sensitivity to environmental stressors, and characteristic feeding behaviour (Morroni et al., 2023). The tropical echinoderm *Astropecten euryacanthus* (Phylum: Echinodermata; Class: Asteroidea; Order: Paxillosida) is a benthic sand star that predominantly inhabits shallow sandy and muddy substrates in tropical and subtropical Indo-Pacific regions, including the coastal waters of the Bay of Bengal (Lütken, 1871). Its coelomocytes are key immunoeffector cells that respond sensitively to environmental stress, and therefore, provide useful cellular biomarkers of contaminant exposure (Pinsino et al., 2008; Smith, 2010). According to Murano et al. (2023), MPs induced alterations in the coelomocyte protein profile of the purple sea urchin *Paracentrotus lividus,* indicating significant disruption of cellular metabolic and functional pathways. A previous study demonstrated that PS-MP exposure can alter coelomocyte abundance and suppress phagocytic activity in the asteroid *Astropecten indicus* (Barua et al., 2021), indicating a morphofunctional shift in coelomocytes exposed to PS-MPs. The decline in coelomocyte count was quantified in the common seastar *Asterias rubens* exposed to environmental stressors (Wahltinez et al., 2023), suggesting immune perturbation in the organism. Enumeration of immunocytes using microscopic analysis and flow cytometry represents a classical biomarker approach for evaluating immunophysiological alterations induced by xenobiotics in experimental models.

Microplastic exposure has been associated with genotoxicity, developmental abnormalities, oxidative damage, and disruption of redox homeostasis in echinoderms (Mazur et al., 2021; Richardson et al., 2021; Murano et al., 2023). The maintenance of redox homeostasis is essential for cellular integrity, whereas immune-related parameters, such as coelomocyte concentration and reactive oxygen species (ROS) production, are established biomarkers of contaminant-induced stress in echinoderms (Coteur et al., 2003). Barua et al. (2021) reported that exposure to PS-MPs and EPS-MPs reduced the activities of antioxidant enzymes, including superoxide dismutase (SOD), catalase (CAT), and glutathione S-transferase (GST) in *A. indicus*, suggesting an impaired capacity to counteract microplastic-induced ROS generation. These alterations highlight antioxidant responses as sensitive biomarkers of ROS-mediated oxidative stress following microplastic exposure. Suspension feeders are particularly susceptible to microplastic ingestion and associated toxicity and may serve as bioindicators for monitoring microplastic pollution in marine ecosystems (Wesch et al., 2016). Collectively, these effects may impair immune and cellular functions, potentially reducing organismal fitness and resilience to environmental stressors.

The present study investigated the immunophysiological responses of the tropical sea star *A. euryacanthus* to PS-MP exposure using an integrated biomarker framework. The novelty of this study lies in the combined application of flow cytometric cell sorting, time-lapse confocal imaging, and an Integrated Biomarker Response (IBR) approach, enabling a complementary assessment of cellular composition, dynamic immune cell responses, and the overall magnitude of toxicological effects. In contrast to previous studies that have predominantly relied on individual or single-endpoint biomarkers, this integrated strategy provides a multidimensional assessment of PS-MP-induced immunotoxicity and addresses the limited mechanistic understanding of the effects of microplastics in tropical asteroids. This approach may further support the development of sensitive coelomocyte-based biomarkers for monitoring microplastic contamination in the Bay of Bengal. Specifically, this study aimed to (1) quantify changes in total and differential coelomocyte abundance following PS-MP exposure, (2) characterise pro-oxidant, oxidative stress, and antioxidant/detoxification responses, and (3) integrate these biomarker responses using the IBR framework to evaluate overall physiological perturbation.

2. Materials and method

2.1. Physicochemical characterisation of PS-MPs

Polystyrene (PS) Styrofoam was collected from a local Indian market, and PS microparticles were prepared mechanically by rubbing the source material over 80-grit sandpaper (NH brand, India). As mechanical abrasion may generate particles with heterogeneous dimensions and morphologies, the physicochemical characteristics of the resulting PS-MPs were assessed using complementary particle-sizing, microscopic, and spectroscopic approaches. Hydrodynamic particle size and surface charge were determined using a Malvern Zetasizer Nano ZS90 (Malvern Instruments Ltd., Worcestershire, U.K.) (El Hadri et al., 2020; Sun et al., 2021). Dynamic light scattering (DLS) analysis revealed a predominant particle size distribution centred at approximately 100 ± 8 nm (Fig. 1B).

The particle morphology and dimensions were examined using a high-resolution field-emission scanning electron microscope (FE-SEM; JEOL JSM-7600F, Japan) operated at 30 kV. The SEM-derived observations were considered complementary to the DLS measurements because DLS estimates the hydrodynamic diameter of particles in suspension, whereas SEM provides direct morphological and dimensional information on individual particles.

Fourier-transform infrared (FTIR) spectroscopy was used to characterise the polymer composition of the microparticles and identify functional groups diagnostic of polystyrene. Spectral analyses were performed using a PerkinElmer Spectrum Two FTIR spectrophotometre equipped with an attenuated total reflectance (ATR) accessory. Measurements were acquired in the mid-infrared region (4000–450 cm^{-1}), with each spectrum generated from an average of 70 co-added scans at a spectral resolution of 4 cm^{-1}. The microparticles were placed directly onto the ATR crystal without chemical or physical pre-treatment to minimise alterations in their surface chemistry. The resulting spectra were processed and interpreted by comparing them with reference polystyrene signatures available in the FTIR spectral library (Kankanige and Babel, 2020).

Raman spectroscopic analysis was performed to corroborate the FTIR-based polymer identification. Raman measurements were conducted at room temperature using a confocal micro-Raman spectrophotometre (LabRAM HR Evolution; HORIBA France SAS) equipped with a Peltier-cooled charge-coupled device (CCD) detector. Spectra were collected over the range of 100–3200 cm^{-1} using a 785-nm diode laser as the excitation source. Spectral validation and cross-referencing were performed using reference Raman spectra from the OpenSpecy polymer database (Ragusa et al., 2022), confirming that the particles were polystyrene.

2.2. Collection, transportation and laboratory acclimation of experimental specimens

Adult, healthy specimens of *A. euryacanthus* were collected from the

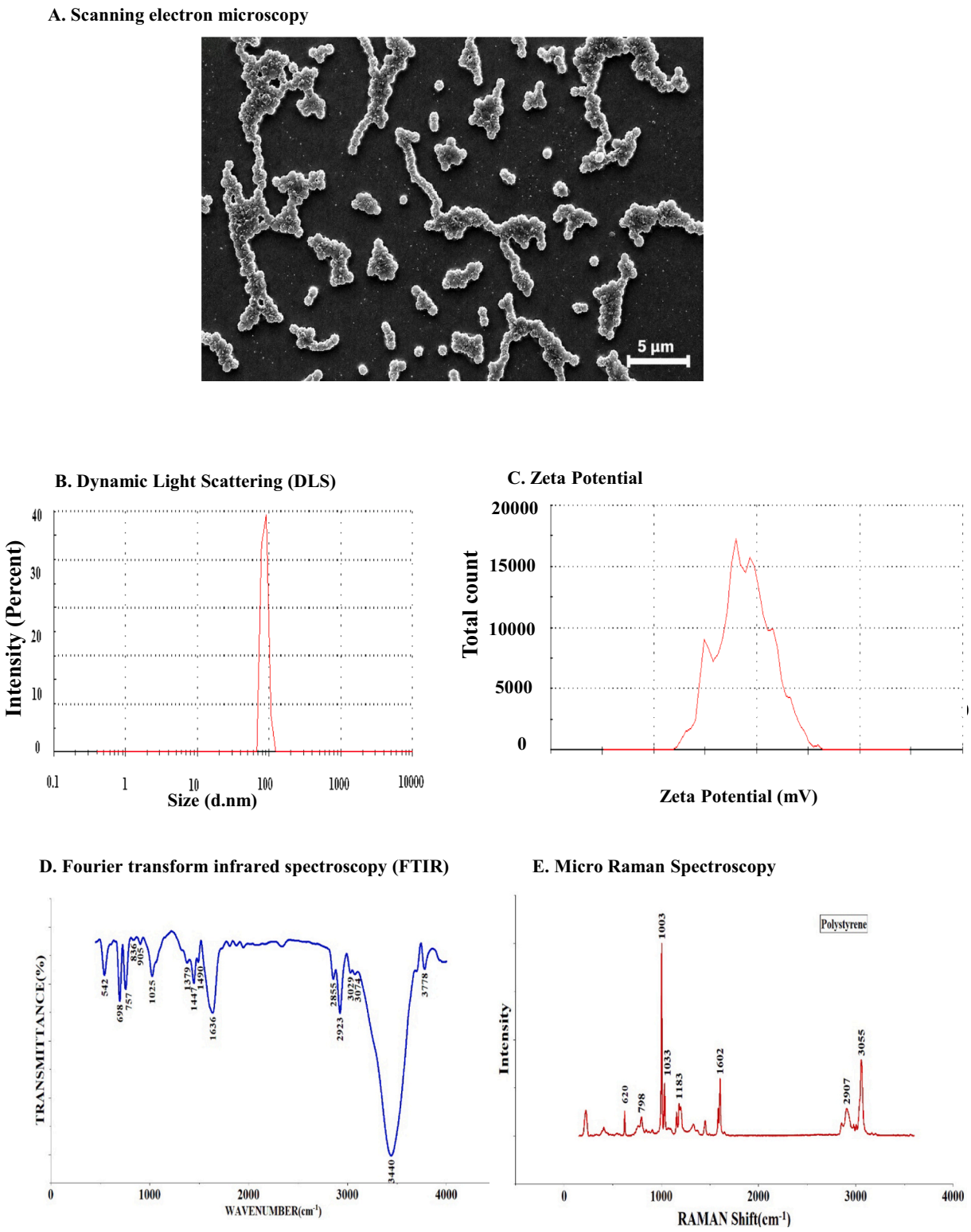


Fig. 1. Physicochemical Characterisation of Polystyrene Microplastics (PS-MPs). Scanning electron microscopy (SEM) (A), dynamic light scattering (DLS) (B), zeta potential analysis (C), Fourier-transform infrared spectroscopy (FTIR) (D), and micro-Raman spectroscopy (E) of PS-MPs used in the exposure experiments. The SEM image illustrates the particle morphology, while the DLS graph represents the particle size distribution. The zeta potential indicates the surface charge characteristics of the particles. FTIR and micro-Raman spectroscopy confirmed the polymeric characteristics of the PS-MPs.

coastal region of West Bengal, India (21.5585°N, 88.2796°E) using net trawling and transported to the laboratory in containers filled with ambient sea water. Individuals with an average body diameter of 4.4 ± 0.3 cm were maintained in glass aquaria containing artificial seawater (ASW) and sand substrate. The aquaria were equipped with continuous aeration and mechanical filtration, with a stocking density of one specimen per 3 L of seawater. Environmental parameters were maintained within stable ranges: temperature 15–22 °C, salinity 33 PSU, and pH 8.0–8.1. The specimens were fed once every 24 h, and the water quality conditions were monitored regularly throughout the acclimation

period. Both acclimation and subsequent experiments were conducted under a controlled 12 h light: 12 h dark photoperiod. In India, the experimental use and handling of marine invertebrates, including echinoderms, are not governed by institutional or national animal ethics regulations; therefore, no ethical approval was required for this study (Barua et al., 2021).

2.3. Experimental design and exposure setup

Adult sea stars were randomly distributed into experimental groups, with each group containing nine individuals ($n = 9$ per container). PS-MPs were administered at three nominal concentrations (0.25, 0.5, and 1 mg/L) for two exposure periods (7 and 14 days). These concentrations were selected to provide a graded exposure range for assessing concentration-dependent response. As the experimental doses may exceed typical field concentrations (Alam et al., 2023), 0.5 and 1 mg/L represent comparatively high particle loads associated with acute or severe pollution events, whereas 0.25 mg/L represents a lower exposure level. Alam et al. (2023) reported an overall microplastic abundance of 3307.22 ± 1732.85 particles kg^{-1} sediment in the Ganges–Meghna river system, with polystyrene accounting for 13.04% of the polymers identified by FTIR, corresponding to an estimated PS-MP abundance of approximately 431 particles kg^{-1} of sediment. A control group maintained under identical conditions without PS-MP addition served as an artificial seawater reference. PS-MP exposure media were prepared by suspending 0.25, 0.5, and 1 mg of particles separately in 1 L of artificial seawater (ASW), corresponding to each nominal concentration of PS-MPs. The suspensions were sonicated for 10 min at 20 °C and 40 W using a Sonics Vibra-Cell VCX 130 sonicator to ensure homogeneity. Exposure solutions were renewed every 24 h with freshly prepared suspensions to minimise particle aggregation, chemical degradation, and accumulation effects during the exposure period. PS-MPs at each concentration were pre-incubated in artificial seawater under the same conditions as the particle exposure, and then filtered to remove particles; the filtrate was used as a leachate-only treatment. Water quality parameters, including pH, alkalinity, and salinity, were routinely monitored in the control and treatment systems to maintain consistent hydrographic conditions. No mortality of *A. euryacanthus* was recorded in any of the treatments throughout the 7- and 14-day exposure periods. Future experiments should complement the present design with environmentally realistic low concentrations and long-term chronic exposures to better resolve responses under sustained field-relevant microplastic contamination.

2.4. Collection and enumeration of coelomocytes of experimental sandstar A. euryacanthus

The coelomic fluid of the experimental sand star was aseptically collected in a sterilised glass vial containing precooled coelomocyte culture medium (CCM: 2 mM EGTA, 20 mM HEPES, 0.5 M NaCl and 5 mM MgCl2, pH 7.9) (Pinsino et al., 2007). The total coelomocyte density was determined microscopically using a Neubauer haemocytometer and expressed as 10^5 cells mL^{-1}. For the estimation of superoxide anion, nitric oxide (NO) generation, flow cytometric count, and preparation of cell lysate, coelomic fluid from five individuals was pooled and centrifuged (Hermle Z323K; Germany) at 4 °C and 650 ×g for 10 min. The pellets were resuspended in 5 mL of CCM and subjected to analysis.

2.5. Flow cytometric analysis of coelomocyte morphotypes

Fresh coelomic fluid was withdrawn from *A. euryacanthus* through the aboral surface using a sterile 26-gauge needle and pre-chilled syringes containing an anticoagulant (calcium–magnesium-free seawater supplemented with 20 mM EGTA). The suspension was passed through a 40 μm cell strainer to remove debris before analysis. Flow cytometry was performed using a BD FACS Aria III fluorescence-activated cell sorter (Becton Dickinson, USA) equipped with a cell sorting module. The instrument operated with a 488 nm blue solid-state laser (20 mW) for scatter signal acquisition and a 633 nm red diode laser (17 mW) for fluorescence detection when required. Coelomocyte populations were resolved based on forward scatter (FSC; cell size) and side scatter (SSC; internal complexity/granularity). A minimum of 50,000 events were recorded per sample. Electronic gating was applied to isolate the target morphotypes and exclude doublets, cellular aggregates, and non-cellular debris. Three distinct coelomocyte fractions were routinely identified and sorted: G1 (small blast-like coelomocytes), G2 (filopodial coelomocytes), and G3 (petalloid coelomocytes). Sorted samples were collected in sterile FACS tubes, centrifuged at 1000 ×*g* for 10 min, and resuspended in PBS for subsequent analyses (Manna et al., 2022). Flow cytometry data were processed using BD FACSDiva 8.0 and FlowJo v10.7. Statistical discrimination of subpopulations was performed using bivariate gating and density contouring methods.

2.6. Cell viability and morphological assessment

Cell viability was evaluated using a 0.4% trypan blue exclusion assay. Viable and non-viable cells were quantified manually using a haemocytometer under bright-field microscopy (Axiostar Plus, Zeiss, Germany). For morphological characterisation, cell suspensions were pipetted onto pre-cleaned glass slides, air-dried for 10 min, and fixed with 70% methanol for 5 min. Giemsa staining (1:20 dilution) was performed for 12–15 min, and the slides were mounted in DPX. A minimum of 200 cells per preparation were examined, and representative photomicrographs were obtained using a CCD imaging system (DGI-510; Dewinter Technologies, Italy).

2.7. Estimation of superoxide anion generation in coelomocytes of sand star A. euryacanthus

Superoxide anion ($O_2\bullet^-$) production in the coelomocytes of *A. euryacanthus* was quantified using the nitroblue tetrazolium (NBT) reduction assay, as described by Takahashi et al. (1993), with modifications. A cell suspension standardised to 1×10^5 cells mL^{-1} was incubated with 0.03% NBT solution for 30 min at 25 °C in the dark to prevent photoreduction. To confirm the assay specificity, an additional SOD-inhibited blank control was included, in which the reaction mixture contained SOD but no test sample. The reduction in the NBT signal in this group was used to verify that the measured signal reflected superoxide-dependent reduction. After incubation, excess NBT was removed by centrifugation at 650 ×*g* for 10 min at 4 °C (Hermle Z323K refrigerated centrifuge, Germany). The reaction was terminated by the addition of 1 mL absolute methanol, followed by washing with 70% methanol to eliminate unbound dye. The intracellular formazan precipitate formed as a result of NBT reduction was dissolved in a mixture of 4 mol L^{-1} KOH and DMSO (1:1, *v*/v) to ensure complete solubilisation of the chromogenic product. The optical density of the solubilised formazan was measured at $\lambda = 630$ nm using a PC-based UV–Vis spectrophotometre (Systronics-119, India). Superoxide generation was expressed as $OD_{630}/(1 \times 10^5$ cells min). The inhibitor control response was compared with the corresponding untreated assay to confirm that the measured NBT reduction was predominantly superoxide-dependent.

$$\text{Superoxide anion generation} = OD_{630}/1 \times 10^5 \text{ cells min}^{-1}$$

This normalisation accounts for cell density and incubation time, enabling a comparative assessment of the oxidative status between the control and polystyrene-exposed specimens.

2.8. Estimation of NO generation by coelomocytes of experimental sand star A. euryacanthus

NO (EC 1.14.13.39) production by *A. euryacanthus* coelomocytes was quantified according to the Griess reaction method described by Green et al. (1982), with modifications for echinoderm cell suspensions. Coelomic cell density was standardised to 1×10^5 cells mL^{-1} in calcium–magnesium-free seawater (CMFS) to minimise spontaneous immune activation. A volume of 1 mL of the standardised suspension was incubated with 1 mL of Griess reagent (0.1% N-(1-naphthyl)ethylenediamine dihydrochloride +1% sulfanilamide in 5% orthophosphoric acid) for 30 min at 25 °C in a humidified chamber under low-light conditions. After incubation, the samples were centrifuged at 650 ×*g* for 5 min at 4 °C (Hermle Z323K, Germany) to remove cellular debris. The supernatant was transferred to cuvettes, and the absorbance was recorded at 550 nm using a PC-based UV–Vis spectrophotometre (Systronics-119, India). The nitrite concentration was determined from a sodium nitrite ($NaNO_2$) calibration curve prepared in the same assay matrix over the range of 0–100 μM. The standard series consisted of 0, 10, 20, 40, 60, 80, and 100 μM $NaNO_2$, and the absorbance of each standard was measured at 550 nm under the same reaction conditions as those of the samples. A linear regression equation was fitted to the standard curve data, and the coefficient of determination (R^2) was recorded for each assay run; only calibration curves exhibiting acceptable linearity ($R^2 \geq 0.99$) were used for sample quantification. The sample NO-equivalent concentrations were interpolated from the regression equation and normalised to the cell number and incubation time.

2.9. Generation of ROS in coelomocyte morphotypes

Intracellular ROS generation in *A. euryacanthus* coelomocytes exposed to PS-MPs for 7 and 14 days was quantified using H2DCFDA (Invitrogen, Thermo Fisher Scientific, UK) and a BD FACSVerse flow cytometer controlled by BD FACSuite software (v1.6). Coelomocytes were standardised to 2×10^5 cells mL^{-1}, incubated with 10 μM H2DCFDA for 30 min at 25 °C in the dark, and passed through a 40-μm nylon mesh before acquisition. The non-fluorescent probe enters the cells and is deacetylated to DCFH, which is oxidised by intracellular ROS, including H_2O_2 and $ONOO^-$, to fluorescent DCF. Therefore, the fluorescence intensity reflects intracellular ROS accumulation. The DCF was excited with a 488-nm laser and detected in the FITC channel using a 532-nm band-pass filter. The instrument performance was standardised using BD FACSuite CS&T Research Beads. FSC and SSC settings were optimised to distinguish the G1, G2, and G3 coelomocyte morphotypes. Samples were acquired at 12 μL min^{-1}, below 500 events s^{-1}, with at least 20,000 single-cell events per sample. Debris and aggregates were excluded using sequential FSC-H versus FSC-A gating, followed by FSC-A, SSC-A, and FL-1 parameters for morphotype identification. Unstained cells served as negative controls for autofluorescence, and reagent-only controls were used to assess background fluorescence and compensation. All instruments and acquisition settings were kept constant across groups. ROS levels were expressed as the geometric mean fluorescence intensity (gMFI) of the gated single-cell population and compared between the control and PS-MP-exposed groups. Data were acquired using BD FACSuite software (v1.6) and analysed with FlowJo (v10.x).

2.10. Detection of ROS generation by confocal laser scanning microscopy

A volume of 150 μL of coelomocyte suspension was incubated with 1× assay binding buffer and DCFDA from the DCFDA ROS Detection Kit (Invitrogen, Thermo Fisher Scientific, UK) for 10 min at room temperature (25 °C) in the dark to prevent photobleaching and premature probe activation. Following incubation, the stained cells were gently mounted onto glass microscope slides, covered with coverslips to avoid air exposure, and immediately examined under differential interference contrast (DIC) and confocal fluorescence optics using a Stellaris Confocal Microscope Platform (Leica Microsystems, UK). Fluorescence was detected from oxidised DCF using 488 nm laser excitation, and emission was collected in the green fluorescence channel corresponding to the DCF.

Time-lapse confocal imaging was performed using the same acquisition settings for all samples. The excitation wavelength was fixed at 488 nm, the detector gain was kept constant at 50%, and images were acquired every 1 min interval for 4 min under the same scanning conditions for all groups. These unified imaging parameters were maintained throughout the experiment and documented with each imaging run to permit valid inter-group comparisons of fluorescence.

2.11. Preparation of cell lysate

Coelomocyte lysates were prepared from pooled cells obtained from experimental starfish. A standardised cell density of 1×10^5 cells mL^{-1} was incubated with 5 mL of 0.1% Triton X-100 on ice at 4 °C for 1 h to ensure complete membrane disruption and the release of intracellular components. Following lysis, the suspension was centrifuged at 650 ×*g* for 15 min at 4 °C using a refrigerated centrifuge (Hermle Z323K, Germany) to remove the cellular debris and insoluble fractions. The resulting supernatant, containing soluble cytosolic enzyme fractions, was carefully collected into pre-chilled glass vials and stored at 4 °C until subsequent biochemical analyses. This lysate was used as the working extract to quantify the activities of key immune and antioxidant enzymes, including phenoloxidase (PO), SOD, CAT, and GST.

2.12. Estimation of activity of PO

PO (EC 1.14.18.1) activity in coelomocyte lysates of *A. euryacanthus* was quantified using L-3,4-dihydroxyphenylalanine (L-DOPA) (Sigma-Aldrich, USA) as the chromogenic substrate, following the method described by Ashida and Söderhäll (1984) with modifications. A volume of 100 μL of enzyme-containing lysate was combined with 200 μL of L-DOPA solution (1.6 mg mL^{-1}) prepared in cacodylate–citrate buffer and incubated for 1 min at room temperature (25 °C) to initiate oxidative reaction. The reaction mixture was subsequently diluted with 20 μL of the same buffer to stabilise the chromogenic product. PO activity was determined by monitoring the formation of dopachrome, and absorbance was measured immediately at 490 nm using a PC-based UV–Vis spectrophotometre (Systronics-119, India). Enzyme activity was normalised to protein concentration (mg $protein^{-1}$) to maintain comparability among samples.

2.13. Estimation of superoxide dismutase activity

SOD (EC 1.15.1.1) activity was estimated as described by Kuthan et al. (1986) with minor modifications. One unit (U) of SOD was expressed as the amount of enzyme required to inhibit the NBT photoreduction rate by 50%. The reaction mixture (2.5 ml of reaction mixture included 50 mM sodium phosphate buffer (pH 7.8), 13 mM methionine, 75 mM NBT, 2 mM riboflavin, 0.1 mM EDTA and 100 μl of coelomocyte lysate. The reaction mixture was kept under two 15 W fluorescent lamps for 15 min, and the reaction was terminated by switching off the lights. A non-irradiated reaction mixture which was continued parallelly with the test, did not develop colour and served as a blank. SOD activity in the coelomocytes of experimental sand stars was estimated spectrophotometrically (Systronics-119, India) at 560 nm, and the enzyme activity was expressed as unit mg $protein^{-1}$ min^{-1}.

2.14. Estimation of CAT activity

CAT (EC 1.11.1.6) activity in coelomocyte lysates of *A. euryacanthus* was quantified following the procedure described by Aebi (1984) with

minor modifications. The rate of hydrogen peroxide (H_2O_2) decomposition was monitored to determine enzyme activity. Briefly, lysate samples were mixed with H_2O_2 substrate solution, and the decrease in H_2O_2 concentration was recorded spectrophotometrically (PC-based UV–Vis spectrophotometre, Systronics-119, India) at 240 nm at 27 °C, corresponding to the absorbance decline associated with substrate breakdown. CAT activity was defined as the amount of enzyme required to reduce the H_2O_2 concentration by 1 μmol min^{-1} under the assay conditions.

2.15. Estimation of GST activity

GST (EC 2.5.1.18) activity in *A. euryacanthus* coelomocyte lysates was quantified according to the method described by Habig et al. (1974), using 1-chloro-2,4-dinitrobenzene (CDNB) as the conjugation substrate. The enzymatic reaction was initiated by the addition of reduced glutathione (GSH) to the assay mixture, and the formation of the GSH-CDNB conjugate was monitored spectrophotometrically at 340 nm using a PC-based UV–Vis spectrophotometre (Systronics-119, India). The assay was performed at 37 °C to maintain optimal catalytic conditions. GST activity was calculated from the increase in absorbance due to conjugate formation and was normalised to the protein concentration. Enzyme activity was expressed as follows:

$$\text{GST activity} = \mu\text{mol conjugate formed} \times \text{mg protein}^{-1} \cdot \text{min}^{-1}$$

indicating the number of micromoles of product formed per minute per milligram of protein under the assay conditions.

2.16. Statistical analyses

All quantitative data obtained from cellular, flow cytometric, and biochemical assays were assessed for compliance with the assumptions of parametric analysis. Normality was evaluated using the Shapiro–Wilk, Anderson–Darling, and Jarque–Bera tests, and homogeneity of variance was assessed using Levene's test. Data satisfying the assumptions of normality and homoscedasticity were analysed using two-way analysis of variance (ANOVA), with PS-MP concentration (control, 0.25, 0.5, and 1 mg/L) and exposure duration (7 and 14 days) as fixed factors. The analysis evaluated the main effects of PS-MP concentration and exposure duration, as well as their concentration × exposure duration interaction. Significant ANOVA effects were followed by Tukey's multiple-comparison test for pairwise comparisons among the treatment groups. Control-leachate comparisons were evaluated separately using the same post-hoc multiple-comparison procedure, where applicable. Statistical analyses were applied to the total coelomocyte count, differential coelomocyte populations, superoxide anion and NO generation, and PO, SOD, CAT, and GST activities. Data are presented as mean ± standard deviation (SD), with $n = 9$ biological replicates per group for each group. Statistical significance was set at $P < 0.05$ (95% confidence level). Analyses and graphical presentations were performed using GraphPad Prism v9.0 (GraphPad Software, USA) and verified using IBM SPSS Statistics v26. (Zhong et al., 2024).

2.17. IBR calculation

The IBR index was calculated following the method described by Beliaeff and Burgeot (2002). The IBR was obtained by integrating the variation in biomarker responses through triangular star-plot areas generated between adjacent biomarkers. For each biomarker, the mean value (m) and standard deviation (s) across all experimental groups were calculated, and the individual biomarker value for each treatment (X) was standardised as $Y = (X - m)/s$, where Y is the standardised biomarker value. Directional correction was applied to account for whether the biomarker response represented activation or inhibition, assigning $Z = Y$ for activation (stimulatory response) and $Z = -Y$ for inhibition (suppressive responses). To avoid negative values during plotting, the minimum *Z*-value for each biomarker was identified, and its absolute value was added to all Z-scores, resulting in the final normalised score $S = Z + |\min Z|$, ensuring $S \geq 0$. The normalised biomarker scores were plotted in a fixed, predefined clockwise order, which was maintained identically for all experimental groups and was not altered according to the treatment response. The indicator sequence used for the IBR star plots was as follows: total coelomocyte count → superoxide anion generation → NO generation → PO activity → SOD activity → CAT activity → GST activity → intracellular ROS generation. These S values were plotted in this sequence on a star diagram, and the triangular areas formed between neighbouring biomarkers were calculated and summed to obtain the final IBR score for each treatment group. IBR values indicate a stronger integrated biological response and higher physiological stress in *A. euryacanthus* following PS-MP exposure.

3. Results

3.1. PS-MP characterisation

Scanning electron microscopy (SEM) revealed a heterogeneous particle morphology, with predominantly irregular and elongated structures of variable dimensions (Fig. 1A). The particle dimensions were evaluated relative to a 5 μm scale bar. Zeta potential analysis indicated a wide surface charge distribution ranging from approximately −100 to +200 mV, suggesting good colloidal stability of the PS-MP suspension (Fig. 1C). FTIR analysis exhibited characteristic absorption bands at 3440, 3074, 3029, 2923, 2855, 1636, 1490, 1447, 1379, 1025, 905, 836, 757 and 698 cm^{-1}. The obtained spectrum was compared with reference spectra from an established FTIR spectral library, and the characteristic peak pattern showed a close match with that of polystyrene (PS) (Fig. 1D). Micro-Raman spectroscopy exhibited characteristic peaks at 620, 798, 1003, 1033, 1183, 1602, 2907, and 3055 cm^{-1}, with a comparison against the Open Specy spectral library demonstrating a characteristic match with polystyrene (Fig. 1E). The observed FTIR and Raman bands corresponded to the characteristic aromatic C—H, C═C, and aliphatic –CH_2– groups of the polystyrene structure, collectively providing a distinct spectral fingerprint for PS. Thus, the concordance of both spectra with their respective reference libraries confirmed the chemical identity of the experimental particles as polystyrene.

3.2. Alteration of coelomocyte abundance and composition

PS-MP exposure significantly altered the total coelomocyte abundance in *A. euryacanthus* (Fig. 2A). At 7 days, total coelomocyte counts increased from 25.50 ± 2.58 × 10^5 cells mL^{-1} in the control to 31.50 ± 3.22, 36.76 ± 4.10, and 38.90 ± 3.88 × 10^5 cells mL^{-1} at 0.25, 0.5, and 1 mg/ L PS-MP, respectively. After 14 days, the corresponding values were 25.50 ± 2.58, 34.70 ± 3.55, 44.20 ± 4.42, and 43.90 ± 4.50 × 10^5 cells mL^{-1}, respectively. Thus, coelomocyte abundance increased progressively with increasing PS-MP concentration, with the strongest elevation occurring at 0.5–1 mg/L concentration. Two-way ANOVA demonstrated significant effects of PS-MP concentration ($F_{(3,64)} = 73.29$, $P < 0.001$) and exposure duration ($F_{(1,64)} = 20.40$, $P < 0.001$) on the total coelomocyte abundance. Importantly, a significant PS-MP concentration × exposure duration interaction was also detected ($F_{(3,64)} = 3.27$, $P = 0.027$), indicating that the magnitude of the coelomocyte response varied between 7 and 14 days depending on the PS-MP concentration.

Flow cytometry resolved three principal populations according to FSC and SSC characteristics: G1 gated blast-like, G2 gated filopodial, and G3 gated petaloid coelomocytes (Fig. 2B). The G1 gated population declined markedly with PS-MP exposure; at 1 mg/L, it decreased to 3.44 ± 0.24% and 2.84 ± 0.18% after 7 and 14 days, respectively. Conversely, G3 increased from 8.87 ± 1.48% and 8.88 ± 1.80% in the corresponding controls to 20.15 ± 2.44% and 19.25 ± 2.05% at 1 mg/L

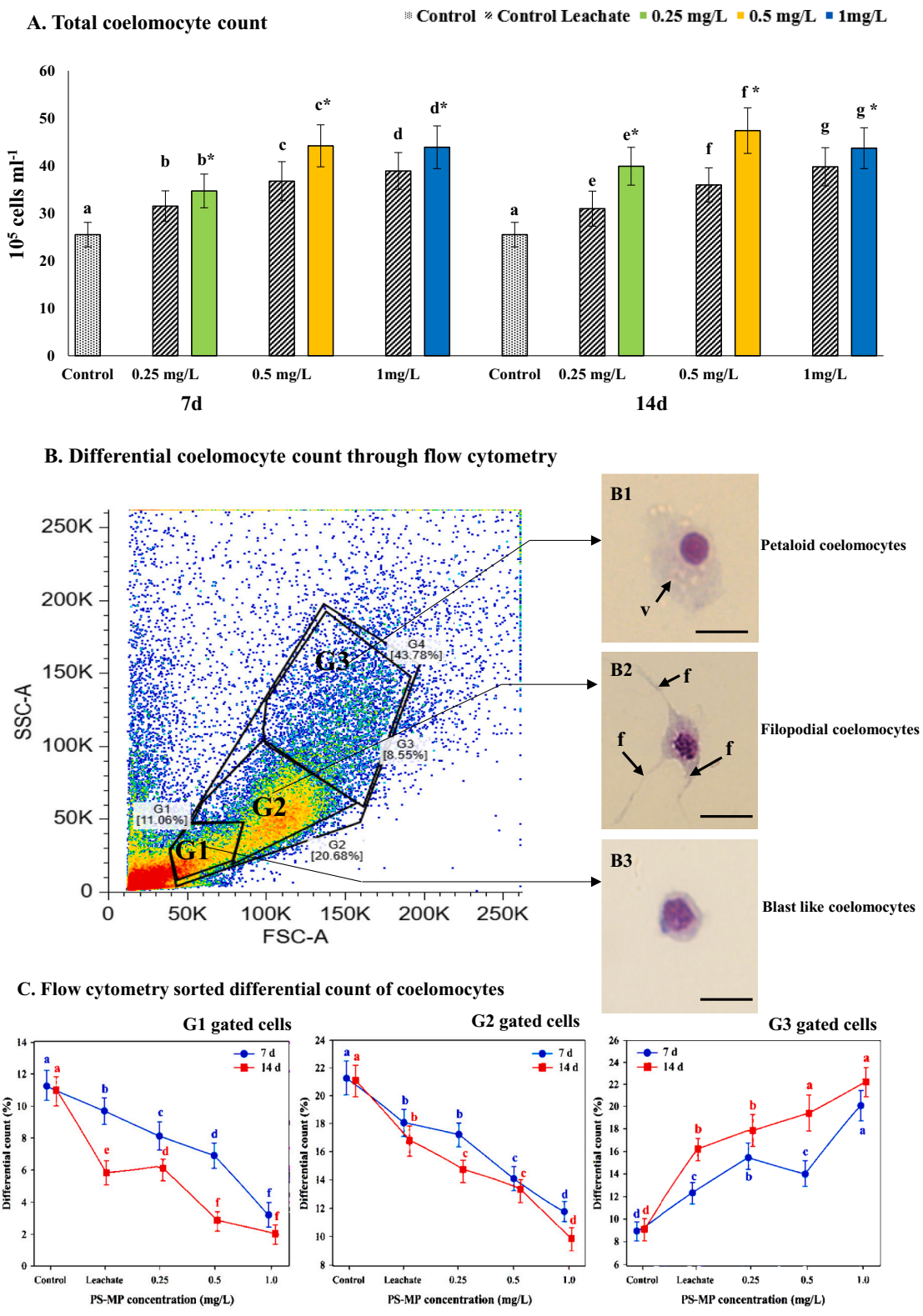


Fig. 2. Effects of PS-MP exposure on total coelomocyte abundance and population composition in *A. euryacanthus*. (A) Total coelomocyte count following exposure to 0.25, 0.5, and 1 mg/LPS-MPs for 7 and 14 days. (B) Representative flow cytometric analysis of coelomocyte populations based on forward scatter (FSC) and side scatter (SSC) characteristics. (B1–B3) Representative light microscopy images of the corresponding coelomocyte morphotypes: petaloid, filopodial, and blast-like cells. (C) Flow cytometry-based differential abundance of the G1, G2, and G3 coelomocyte populations after 7 and 14 days exposure. G1, G2, and G3 represent the three principal flow cytometrically resolved coelomocyte populations. Data are presented as mean ± SD ($n = 9$). Statistical significance was evaluated using two-way analysis of variance (ANOVA), followed by Tukey's multiple comparison test. Different lowercase letters indicate significant differences among experimental groups across PS-MP concentrations and exposure durations (7 and 14 days). Groups sharing similar letters and symbols (*) are not significantly different. Statistical significance was set at $P < 0.05$. f = filopodia, v = vacuole.

(Fig. 2C). G1 gated coelomocyte abundance decreased significantly with increasing PS-MP concentration, reaching its lowest level at 1 mg/L at both exposure durations. This reduction was further significant after 14 days, indicating sustained depletion of this population. In contrast, G3 gated coelomocyte abundance increased significantly across the exposure gradient, with the highest proportion occurring at 1 mg/L; however, its proportion was slightly lower after 14 days than after 7 days at the highest concentration. G2 gated coelomocyte also exhibited a significant concentration-dependent redistribution, with the response differing between exposure durations. Collectively, these statistically significant shifts demonstrate that PS-MP exposure altered the relative composition of coelomocyte populations rather than simply reducing the total cell abundance, suggesting a concentration- and duration-dependent redistribution of immune cell phenotypes. Therefore, the response represents a dose-responsive redistribution of coelomocyte subpopulations rather than a uniform reduction in cellular abundance.

3.3. Shift in pro-oxidant and immune effector responses

PS-MP exposure significantly altered prooxidant responses in the coelomocytes of *A. euryacanthus* (Fig. 3). Superoxide anion generation increased progressively with increasing PS-MP concentration. At 7 days, superoxide anion generation increased from 0.115 ± 0.0066 OD 10^5 cells^{-1} min^{-1} in the control to 0.161 ± 0.0078, 0.174 ± 0.0079, and 0.184 ± 0.0060 OD 10^5 cells^{-1} min^{-1} at 0.25, 0.5, and 1 mg/L, respectively. After 14 days, the corresponding values were 0.117 ± 0.0065, 0.164 ± 0.0075, 0.175 ± 0.0097, and 0.189 ± 0.0061 OD 10^5 cells^{-1} min^{-1} for control, 0.25, 0.5, and 1 mg/L, respectively. Two-way ANOVA revealed a highly significant effect of PS-MP concentration ($F_{(3,64)} = 316.74$, $P < 0.001$), whereas exposure duration ($F_{(1,64)} = 2.52$, $P = 0.118$) and concentration × duration interaction ($F_{(3,64)} = 0.24$, $P = 0.866$) were not significant.

NO generation exhibited a concentration- and duration-dependent pattern of generation. At 7 days, NO levels were 0.0135 ± 0.00086, 0.0188 ± 0.00094, 0.0104 ± 0.00080, and 0.0193 ± 0.00113 for control, 0.25, 0.5, and 1 mg/L PS-MP, respectively. Following 14 days exposure, the respective values were 0.0137 ± 0.00085, 0.0117 ± 0.00091, 0.0172 ± 0.00087, and 0.0180 ± 0.00089. Two-way ANOVA demonstrated significant effects of PS-MP concentration ($F_{(3,64)} = 100.86$, $P < 0.001$) and a significant concentration × exposure duration interaction ($F_{(3,64)} = 194.35$, $P < 0.001$), whereas the main effect of exposure duration was not significant ($F_{(1,64)} = 0.14$, $P = 0.714$). Thus, the NO response varied significantly between exposure durations, depending on the PS-MP concentration.

PO activity was also significantly affected by PS-MP exposure. At 7 days, PO activity decreased from 0.65 ± 0.0276 in the control to 0.34 ± 0.020, 0.51 ± 0.024, and 0.43 ± 0.027 at 0.25, 0.5, and 1 mg/L, respectively. After 14 days, PO activity was 0.63 ± 0.0276, 0.32 ± 0.022, 0.49 ± 0.039, and 0.45 ± 0.026 for control, 0.25, 0.5, and 1 mg/L, respectively. Two-way ANOVA indicated a significant effect of PS-MP concentration ($F_{(3,64)} = 406.73$, $P < 0.001$), whereas neither exposure duration ($F_{(1,64)} = 2.44$, $P = 0.123$) nor the concentration × duration interaction ($F_{(3,64)} = 2.44$, $P = 0.073$) was significant. Therefore, the reduction in PO activity was primarily associated with PS-MP concentration rather than exposure duration.

Collectively, the three biomarkers demonstrated that PS-MP exposure produced marked alterations in prooxidant and immune-associated biochemical responses, characterised by enhanced SOA generation, concentration- and duration-dependent modulation of NO production, and reduced PO activity. The concentration × duration interaction was particularly evident for NO, whereas SOA and PO responses remained comparatively consistent between the two exposure periods. The experimental design comprised control and three PS-MP concentrations evaluated after 7 and 14 days, with data expressed as mean ± SD ($n = 9$).

3.4. Cell-type-specific intracellular ROS generation

Flow cytometric DCF fluorescence revealed distinct ROS responses among the three coelomocyte populations (Fig. 4). After 7 days, G1 fluorescence increased from 4400 ± 380 median DCF units in controls to 6200 ± 520, 8345 ± 698, and 9754 ± 890 at 0.25, 0.5, and 1 mg/L, respectively. G3 exhibited a similar concentration-related increase, from 1300 ± 130 in controls to 1654 ± 145, 2354 ± 345, and 2754 ± 321 median DCF units (Fig. 4B).

After 14 days, the response became nonlinear. G1 reached 9444 ± 800 median DCF units at 1 mg/L, whereas G2 reached 21,005 ± 2190 median DCF units at the same concentration. In contrast, G3 gated coelomocytes exhibited its maximum response at 0.5 mg/L (2486 ± 250 median DCF units) rather than at 1 mg/L (Fig. 4B).

Thus, prolonged PS-MP exposure produced cell-type-specific and non-linear oxidative responses, indicating that exposure duration modifies rather than simply amplifies the concentration response.

PS-MP exposure induced distinct cell type-specific patterns of ROS generation in *A. euryacanthus* coelomocytes. At 7 days, the median DCF fluorescence increased progressively with PS-MP concentration in the G1, G2, and G3 populations, with the most pronounced response observed in the G1 blast-like coelomocytes. G3 petaloid cells exhibited comparatively higher basal ROS levels, but only a slight increase. After 14 days, all three populations displayed nonlinear responses, with a peak at approximately 0.5 mg/L followed by a decline at 1 mg/L, indicating a time-dependent shift from concentration-responsive oxidative activation toward an adaptive response (Fig. 4 A3, B).

3.5. Confocal validation and temporal progression of ROS

Confocal microscopy confirmed the spatial distribution of intracellular ROS formation. In Fig. 6, DIC images are presented in A1, B1, and C1; the corresponding DCF-positive cells are displayed in A2, B2, and C2; and merged images are displayed in A3, B3, and C3. Green intracellular fluorescence confirmed the presence of ROS-associated DCF signals in PS-MP-exposed coelomocytes.

Time-lapse imaging further demonstrated progressive fluorescence accumulation following a 14-day exposure to 1 mg/L PS-MPs (Fig. 7A, B). Fluorescence increased continuously over the 240-s observation period, with individual cells reaching approximately 20,000–28,000 arbitrary fluorescence units. Variations among the tracked cells indicate heterogeneity in cellular oxidative responsiveness.

These observations provide temporal evidence of sustained intracellular DCF accumulation, complementing endpoint measurements obtained by flow cytometry.

3.6. Perturbation of antioxidant defense

SOD activity was significantly suppressed after PS-MP exposure (Fig. 5A). After 7 days, SOD activity decreased from 0.138 ± 0.0065 unit mg protein^{-1} min^{-1} in the control to 0.112 ± 0.0063, 0.0945 ± 0.0050, and 0.106 ± 0.0062 unit mg protein^{-1} min^{-1} at 0.25, 0.5, and 1 mg/L, respectively. The strongest inhibition occurred at 0.5 mg/L, followed by partial recovery at 1 mg/L, indicating a non-monotonic concentration response relationship. After 14 days, SOD activity remained lower than that of the control, with values of 0.140 ± 0.0064, 0.104 ± 0.0055, 0.0967 ± 0.0067, and 0.118 ± 0.0059 unit mg protein^{-1} min^{-1} for the control, 0.25, 0.5, and 1 mg/L treatments, respectively. Two-way ANOVA revealed a significant effect of PS-MP concentration ($F_{(3,64)} = 162.50$, $P < 0.001$) and a significant concentration × exposure duration interaction ($F_{(3,64)} = 8.10$, $P < 0.001$), whereas the main effect of exposure duration was not significant ($F_{(1,64)} = 2.04$, $P = 0.158$). This significant interaction indicates that the SOD suppression pattern differed between 7 and 14 days across PS-MP concentrations.

CAT activity was altered following PS-MP exposure (Fig. 5B). After 7 days, CAT activity decreased from 0.0083 ± 0.0004 k mg

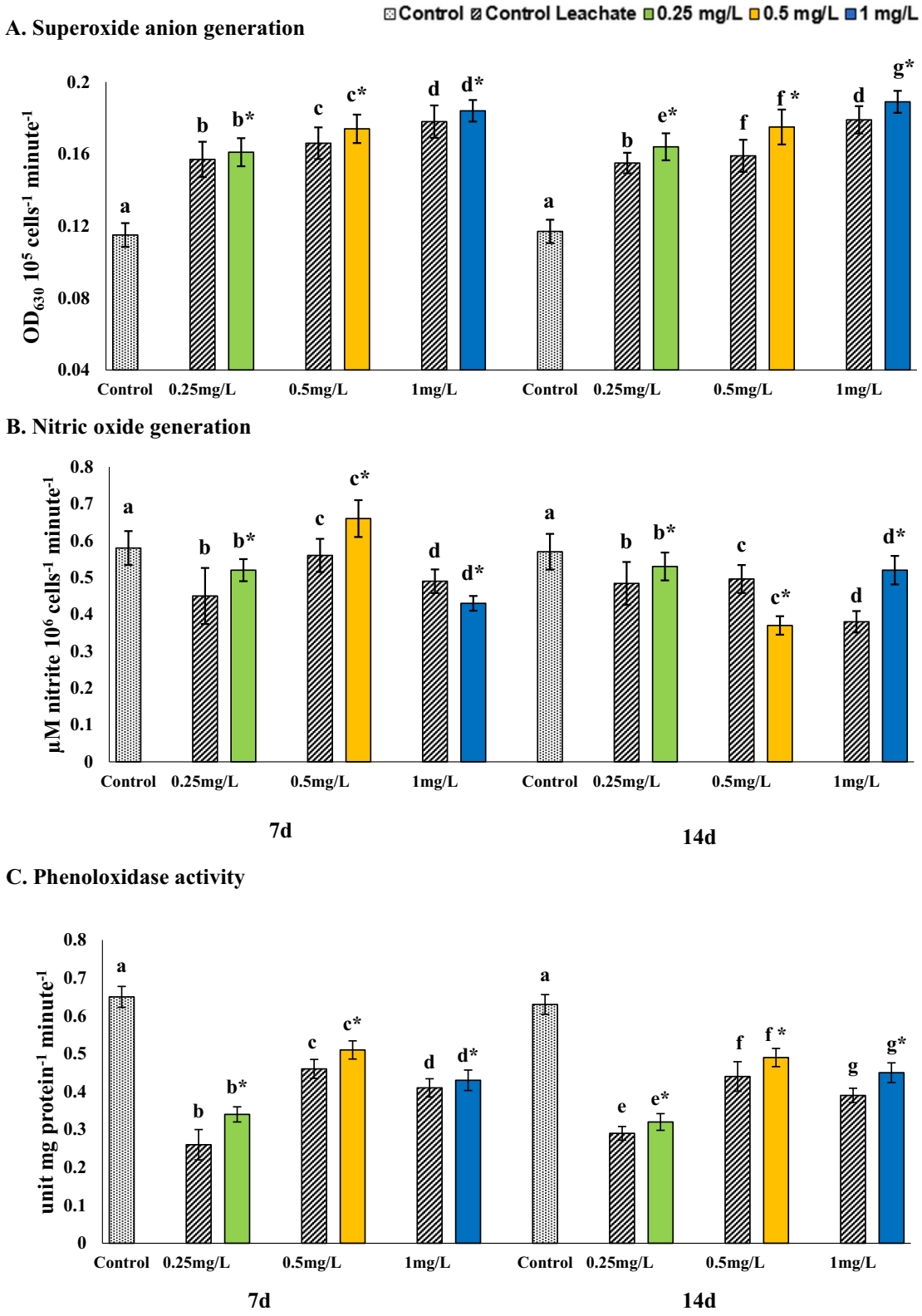
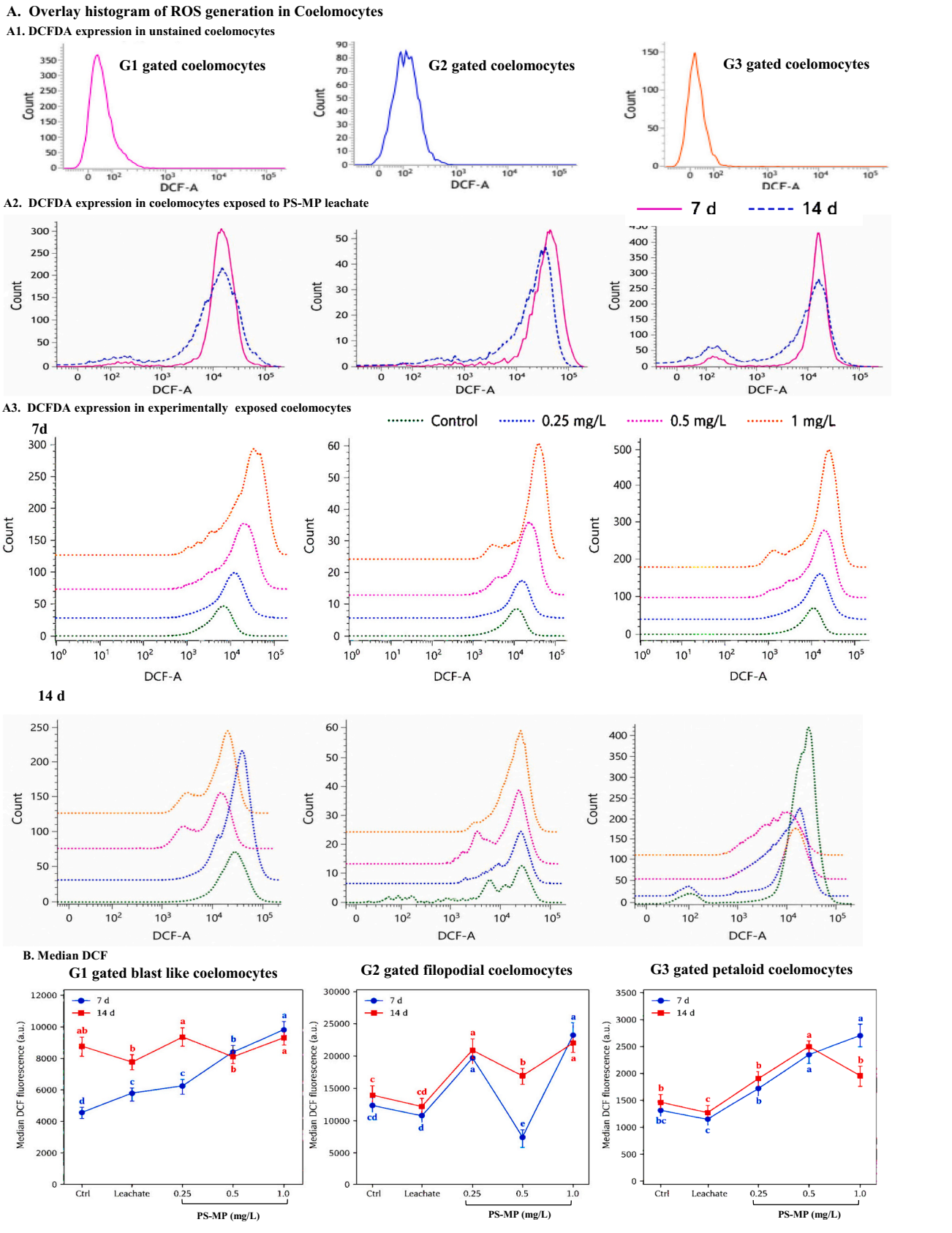


Fig. 3. Effects of PS-MP exposure on prooxidant and phenoloxidase responses in the coelomocytes of *A. euryacanthus*. (A) Superoxide anion ($O_2^{-}\bullet$) generation, (B) nitric oxide (NO) generation, and (C) phenoloxidase (PO) activity in coelomocytes following exposure to 0.25, 0.5, and 1 mg/LPS-MPs for 7 and 14 days. Data are presented as mean ± SD ($n = 9$). Statistical significance was evaluated using two-way ANOVA with PS-MP treatment and exposure duration as factors, followed by Tukey's multiple comparison test. Asterisks (*) denote significant differences between the PS-MP-exposed groups and the control and control-leachate groups, whereas different lowercase letters denote significant differences among the PS-MP concentrations and exposure durations. Statistical significance was accepted at $P < 0.05$.



(caption on next page)

Fig. 4. Cell-type-specific intracellular reactive oxygen species (ROS) generation in *A. euryacanthus* coelomocytes following PS-MP exposure. (A) Overlay histograms of 2′,7′-dichlorofluorescein diacetate (DCFDA)-derived fluorescence in G1-, G2-, and G3-gated coelomocytes. The histograms include (A1) unstained coelomocytes, (A2) coelomocytes exposed to control leachate, and (A3) PS-MP-exposed coelomocytes. The first and second columns represent 7- and 14-d exposure, respectively. (B) Median DCF fluorescence intensity of G1-, G2-, and G3-gated coelomocytes corresponding to blast-like, filopodial, and petaloid morphotypes, respectively, exposed to 0.25, 0.5, and 1 mg/LPS-MPs. Data are presented as mean ± SD ($n = 9$). Statistical significance was evaluated using two-way ANOVA with treatment and exposure duration as factors, followed by Tukey's multiple comparison test. Different lowercase letters indicate significant differences among the experimental groups within each exposure period (7 and 14 days). Blue and red letters denote statistical groupings for the 7- and 14-d exposures, respectively; groups sharing a letter are not significantly different. Statistical significance was set at $P < 0.05$. DCF fluorescence represents intracellular oxidant-sensitive fluorescence, which was detected using flow cytometry. Ctrl = Control. (For interpretation of the references to colour in this figure legend, the reader is referred to the web version of this article.)

protein^{-1} min^{-1} in the control to 0.0072 ± 0.0005, 0.0069 ± 0.00055, and 0.0061 ± 0.00062 k mg protein^{-1} min^{-1} at 0.25, 0.5, and 1 mg/L PS-MP, respectively. After 14 days, CAT activity was 0.0081 ± 0.00041 k mg protein^{-1} min^{-1} in the control and declined to 0.00713 ± 0.00050, 0.0067 ± 0.00047, and 0.0062 ± 0.00049 k mg protein^{-1} min^{-1} at 0.25, 0.5, and 1 mg/L, respectively. Thus, CAT activity exhibited a concentration-dependent decline, with the greatest reduction occurring at 1 mg/L for both exposure durations. Two-way ANOVA revealed a significant effect of PS-MP concentration on CAT activity ($F_{(3,64)} = 53.56$, $P < 0.001$), whereas the main effect of exposure duration was not significant ($F_{(1,64)} = 0.62$, $P = 0.433$). The PS-MP concentration × exposure duration interaction was also not significant ($F_{(3,64)} = 0.37$, $P = 0.776$), indicating that the concentration-dependent reduction in CAT activity was broadly consistent between 7 and 14 days.

GST activity displayed a contrasting pattern, with progressive induction following PS-MP exposure (Fig. 5C). After 7 days, GST activity increased from 0.0218 ± 0.0012 μmol mg protein^{-1} min^{-1} in the control to 0.0246 ± 0.0014, 0.0283 ± 0.0019, and 0.0301 ± 0.0021 μmol mg protein^{-1} min^{-1} at 0.25, 0.5, and 1 mg/L, respectively. After 14 days, GST activity increased further to 0.0269 ± 0.0018, 0.0314 ± 0.0022, and 0.0346 ± 0.0025 μmol mg protein^{-1} min^{-1} at the corresponding PS-MP concentrations, whereas the control remained at 0.0218 ± 0.0012 μmol mg protein^{-1} min^{-1}. Two-way ANOVA indicated a significant effect of PS-MP concentration ($F_{(3,64)} = 114.01$, $P < 0.001$) and exposure duration ($F_{(1,64)} = 32.44$, $P < 0.001$). A significant PS-MP concentration × exposure duration interaction was also detected ($F_{(3,64)} = 4.70$, $P = 0.005$), demonstrating that GST induction became progressively stronger with prolonged exposure.

Collectively, the antioxidant responses demonstrate the differential regulation of the cellular defense system under PS-MP exposure. SOD was suppressed in a non-monotonic manner, CAT exhibited a concentration- and time-dependent alteration, whereas GST was progressively induced, with stronger responses after 14 days. The significant concentration × duration interactions for SOD and GST indicate that the exposure duration modified the response to the PS-MP concentration rather than simply amplifying the effect.

3.7. Integrated biomarker response

The integrated biomarker response (IBR/n) was calculated from the standardised biomarker responses using the triangular star-plot approach of Beliaeff and Burgeot (2002). The analysis integrated the total coelomocyte count, pro-oxidant activity, oxidative stress/ROS response, and antioxidant-related biomarkers. The standardised biomarker profiles are presented as star plots in Fig. 8A–C, with the corresponding integrated IBR/n analysis displayed in Fig. 8D. The IBR/n values were 1 for the control, 0.68 at 0.25 mg/L, 0.82 at 0.5 mg/L, and 0.99 at 1 mg/L (Fig. 8D). The lower IBR/n at 0.25 mg/L indicates a comparatively smaller integrated deviation across the biomarker suite, whereas the increase to 0.82 at 0.5 mg/L indicates a greater cumulative alteration of the measured immune and redox endpoints. At 1 mg/L, IBR/n further increased to 0.99, approaching the control value of 1, suggesting that the integrated response did not follow a simple monotonic concentration–response relationship. Rather, the IBR profile indicated a concentration-dependent shift in the relative contribution of individual biomarkers, with the highest PS-MP concentration producing an overall biomarker configuration similar in magnitude to the control, despite substantial alterations in individual endpoints (Fig. 8A–D).

Since conventional IBR/n integrates multiple standardised endpoints into a single descriptive index and does not retain the individual biological variability required for direct inferential comparison among treatments, these values should be interpreted as an integrated response pattern rather than independent evidence of statistically significant differences (Fig. 8D). Thus, the IBR analysis complements the individual biomarker results by demonstrating that PS-MP exposure produced a multidimensional and non-linear alteration of immune and redox status, rather than a uniformly increasing overall stress response.

4. Discussion

4.1. PS-MP-induced modulation of coelomocyte homeostasis

The present study demonstrates that PS-MP exposure markedly modulates coelomocyte homeostasis in *A. euryacanthus*, as evidenced by increased total coelomocyte abundance and redistribution of the G1–G3 gated cellular populations. The concentration-dependent increase in total coelomocyte abundance indicates an active cellular response to particle exposure and suggests mobilisation of circulating immune cells. Coelomocytes are fundamental components of echinoderm innate immunity and participate in particle recognition, phagocytosis, cytotoxicity, encapsulation, and cellular defense. Therefore, changes in their abundance and population structure provide informative cellular-level signatures of environmental stress.

Previous studies on the congeneric benthic sea star *A. indicus* demonstrated that PS-MPs and expanded PS-MPs can alter coelomocyte abundance, phagocytic activity, prooxidant production, and antioxidant responses. Barua et al. (2021) further demonstrated that PS-MPs affect coelomocyte function at concentrations of 0.5 and 1 mg/L, with expanded PS-MPs producing stronger cytotoxic and oxidative responses. The consistency between these observations and the present results supports the responsiveness of *Astropecten* coelomocytes to PS-MP exposure.

Flow cytometry further demonstrated that increased total cell abundance was accompanied by a shift in cellular composition. The reduction in G1-gated coelomocytes together with enrichment of G3 cells suggests redistribution among morphologically distinguishable coelomocyte states during exposure. The increase in G3-gated coelomocytes may represent mobilisation of cells involved in active immune defense, whereas the reduction in G1 cells may reflect utilisation or redistribution of this population. However, echinoderm coelomocyte categories should primarily be interpreted according to their morphological and functional characteristics rather than as rigid developmental lineages (Queiroz and Custódio, 2025). Comparable alterations in immune-related parameters following microplastic exposure have also been reported in yellowfin seabream, where microplastic exposure altered immune responses and induced DNA damage (Shirmohammadi et al., 2025).

The present findings are also consistent with observations in *Paracentrotus lividus*, where PS microbeads increased total immune cell abundance and altered intracellular reactive oxygen and nitrogen

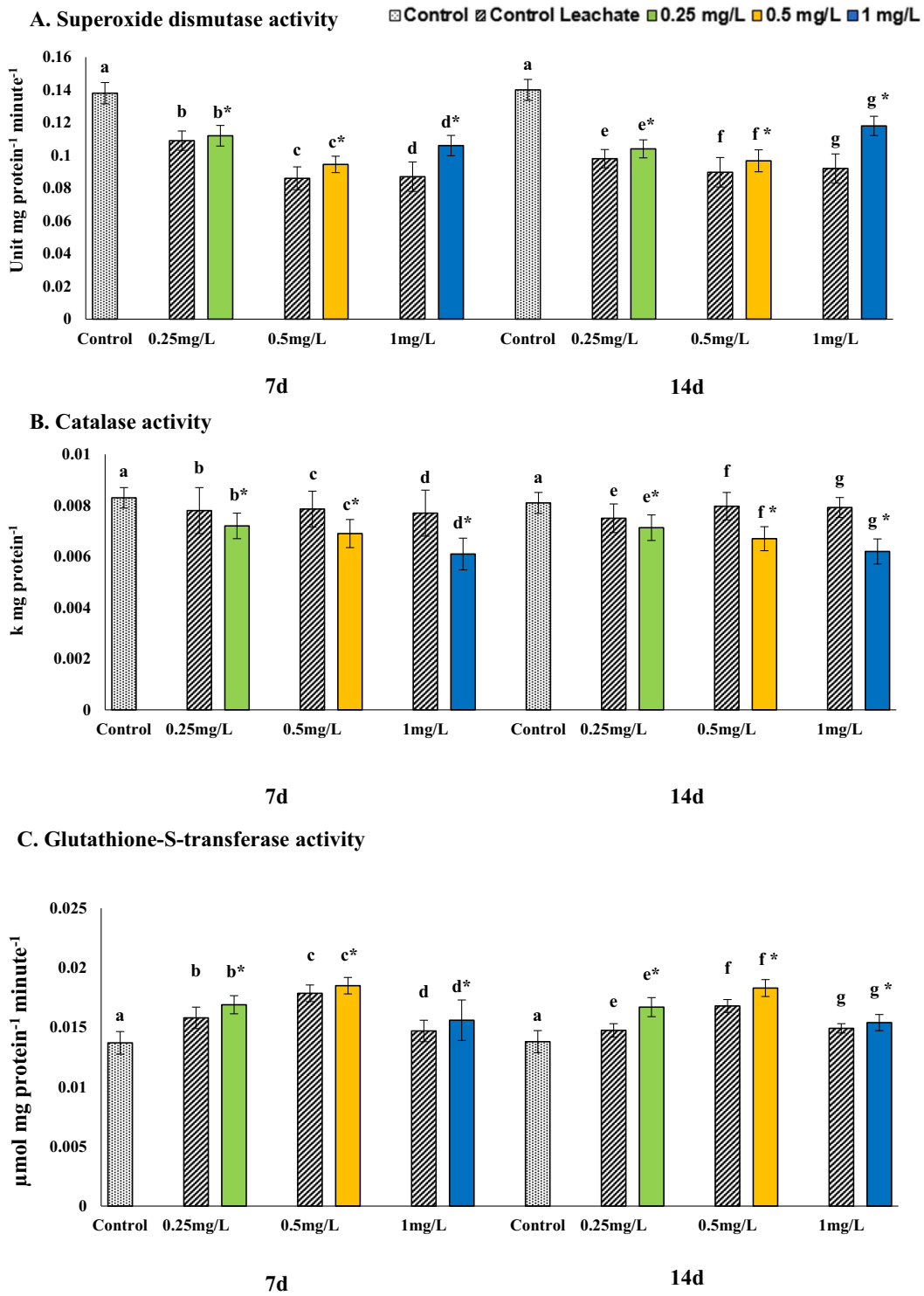


Fig. 5. Effects of PS-MP exposure on antioxidant and detoxification enzyme activities in *A. euryacanthus* coelomocyte. (A) Superoxide dismutase (SOD), (B) catalase (CAT), and (C) glutathione-S-transferase (GST) activities following exposure to 0.25, 0.5, and 1 mg/LPS-MPs for 7 and 14 days. Data are presented as mean ± SD ($n = 9$). Statistical significance was evaluated using two-way ANOVA with PS-MP treatment and exposure duration as factors, followed by Tukey's multiple comparison test. Asterisks (*) denote significant differences between PS-MP-exposed groups and the control and control-leachate groups, while different lowercase letters denote significant differences among PS-MP concentrations and exposure durations. Statistical significance was accepted at $P < 0.05$. The plotted datasets comprise the concentration- and duration-dependent responses of SOD, CAT, and GST, as displayed in panels A–C. The unit of CAT is expressed as first order rate constant (k) per mg protein.

species (Murano et al., 2020). More recently, Murano et al. (2023) demonstrated concentration-dependent changes in the immune cell proteome of *P. lividus* following PS-MP exposure, particularly in pathways related to cellular metabolism and biochemical processes. Thus, the present study extends evidence of PS-MP-responsive immune-cell alterations across echinoderms to a tropical benthic asteroid.

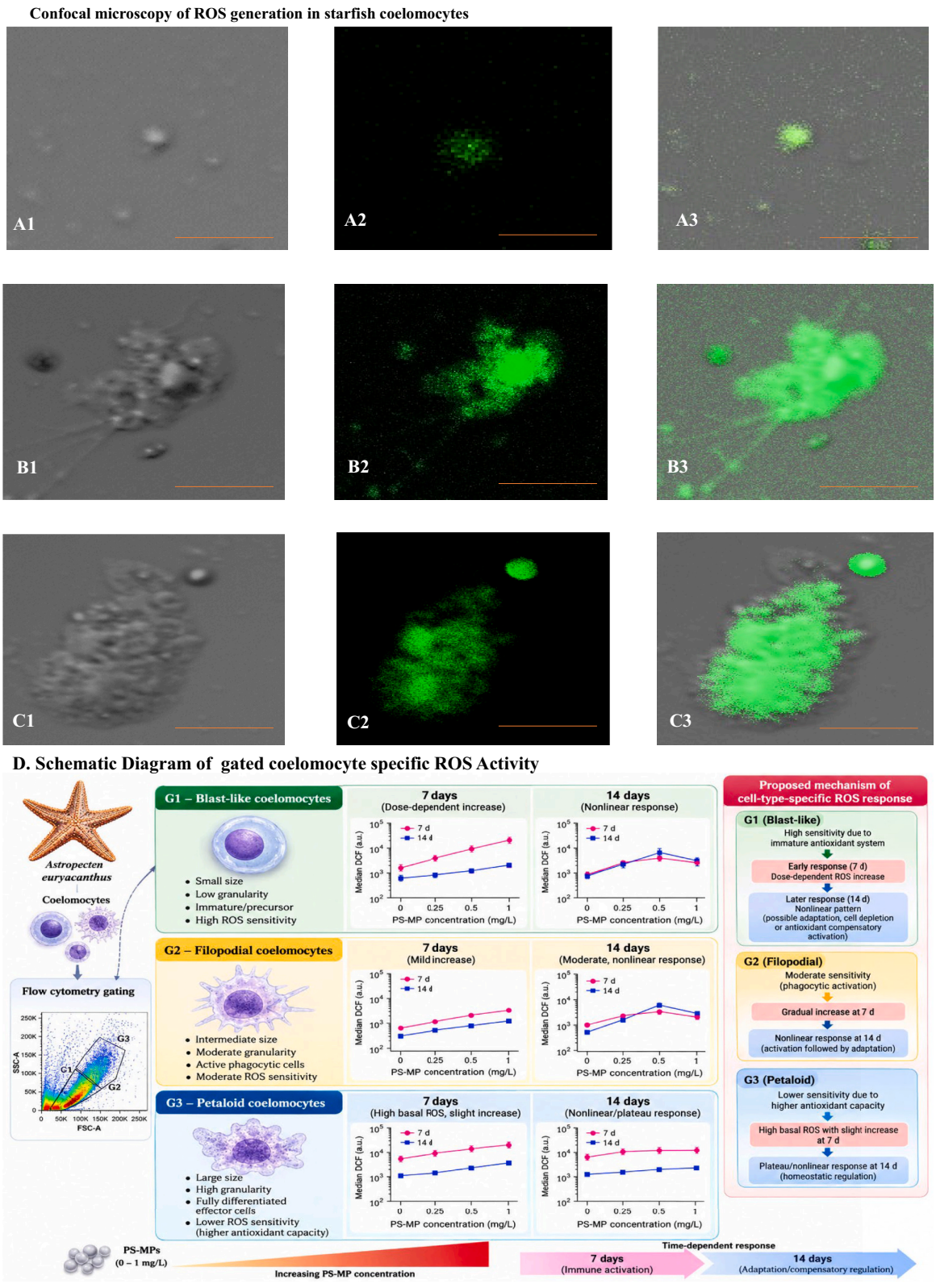
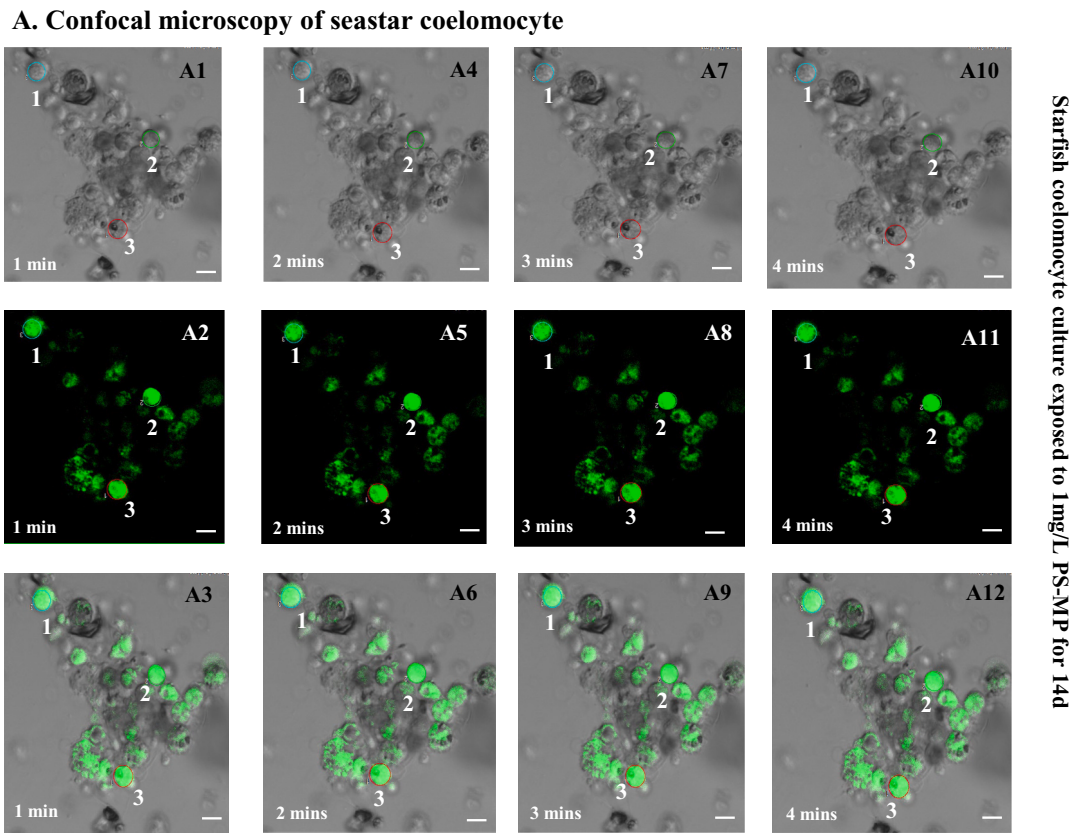


Fig. 6. Confocal immunofluorescence detection of intracellular ROS in *A. euryacanthus* coelomocytes following DCFDA staining. Differential interference contrast (DIC) images are displayed in panels A1, B1, and C1, corresponding to the control, 1 mg/L PS-MP exposure for 7 days, and 1 mg/L PS-MP exposure for 14 days, respectively. Corresponding DCF-positive coelomocytes exhibiting green fluorescence are presented in A2, B2, and C2, respectively, while merged DIC and fluorescence images are displayed in A3, B3, and C3, respectively. Green fluorescence represents intracellular oxidant-sensitive DCF accumulation following DCFDA staining. Scale bar = 50 μm.

(D) Schematic representation of flow cytometric discrimination of three morphologically distinguishable coelomocyte populations (G1 gated blast-like, G2 gated filopodial, and G3 gated petaloid coelomocytes) with their corresponding median DCF fluorescence responses following exposure to 0, 0.25, 0.5, and 1 mg/L PS-MPs for 7 and 14 days. (For interpretation of the references to colour in this figure legend, the reader is referred to the web version of this article.)



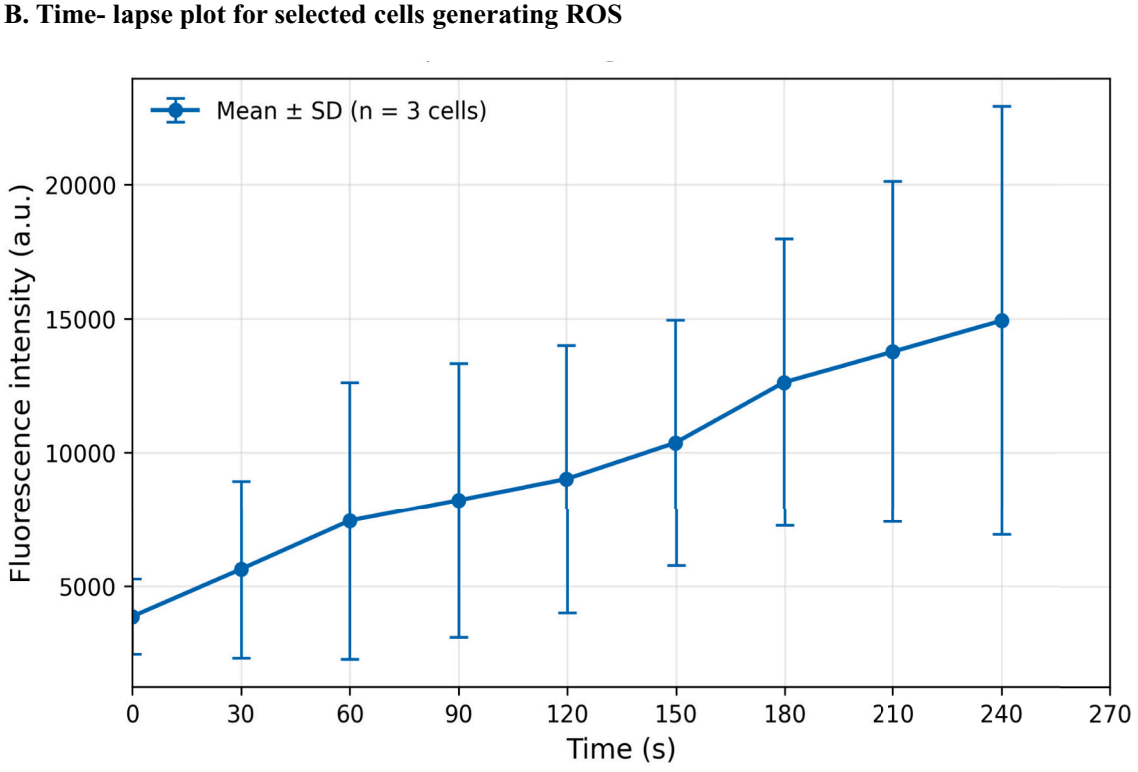


Fig. 7. Time-resolved confocal imaging of intracellular ROS accumulation in *A. euryacanthus* coelomocytes. (A) Representative time-lapse confocal images of coelomocytes exposed to 1 mg/LPS-MPs for 14 days, stained with DCFDA, and imaged at 1, 2, 3, and 4 min. DIC images are displayed in A1, A4, A7, and A10; the corresponding DCF-positive fluorescence images are displayed in A2, A5, A8, and A11; and the merged images are displayed in A3, A6, A9, and A12. (B) Temporal changes in DCF fluorescence intensity in three selected coelomocytes during the 4-min observation period. Data are presented as mean ± SD ($n = 3$). Time-lapse analysis illustrated the progressive accumulation of oxidant-sensitive DCF fluorescence and cell-to-cell variability in the oxidative response.

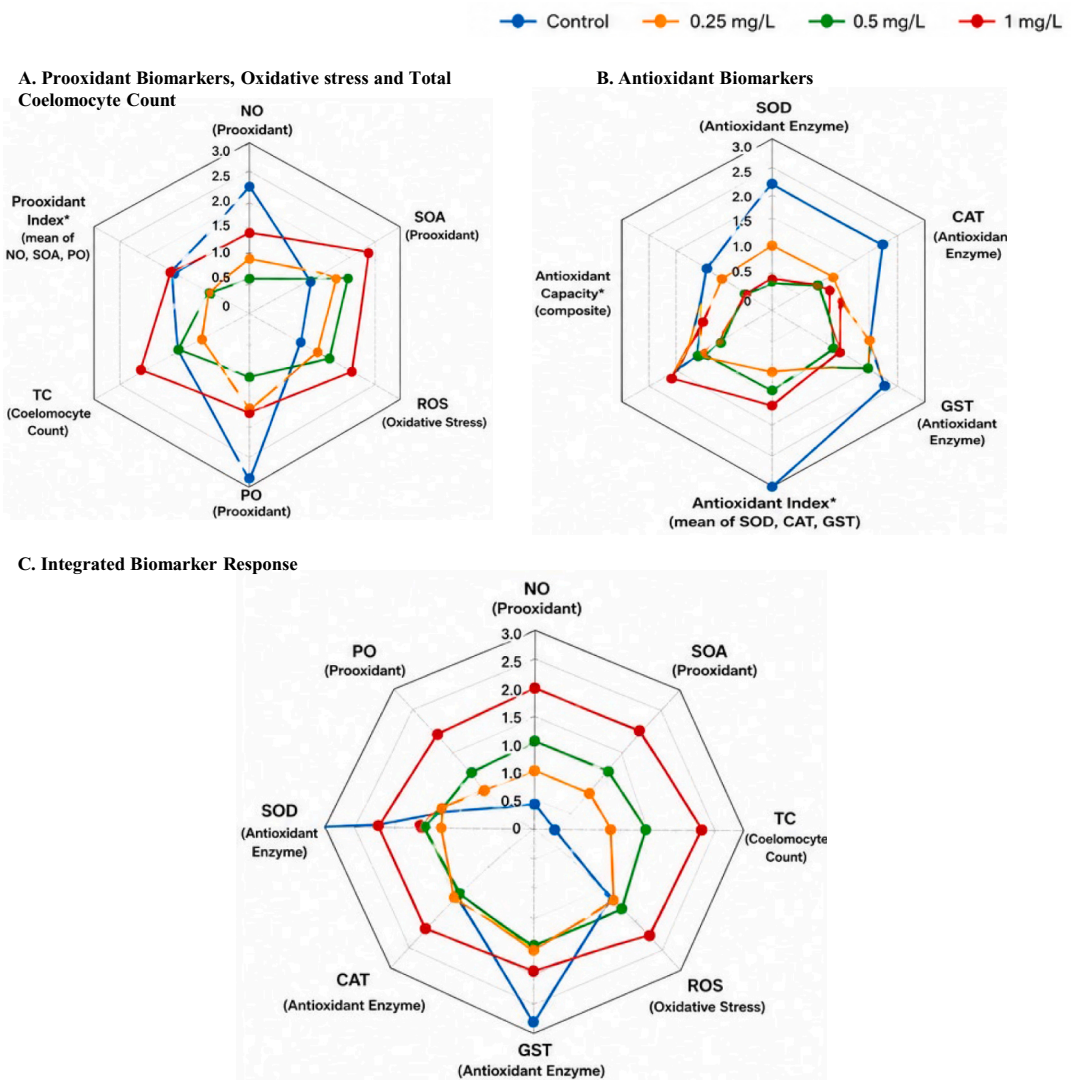


Fig. 8. Integrated biomarker response (IBR) analysis of PS-MP-induced immune and redox perturbations in *A. euryacanthus*. (A) Standardised responses of total coelomocyte count and prooxidant/oxidative stress biomarkers; (B) standardised antioxidant and detoxification biomarker responses; (C) integrated biomarker response profiles generated from the standardised biomarker scores; and (D) normalised integrated biomarker response (IBR/n) across PS-MP treatments. Biomarker responses were standardised relative to the overall mean and standard deviation, followed by a directional adjustment according to the biological relevance of each endpoint. The biomarkers were arranged in a fixed clockwise sequence for the IBR calculation. For adjacent standardised scores (S_i and S_{i+1}), the contribution of each segment was calculated as $A_i = [(S_i + S_{i+1})/2] \times |S_{i+1} - S_i|$, and the IBR was obtained by summing the areas of all the adjacent segments. IBR/n was calculated by dividing the IBR by the number of biomarkers included in the analysis. Higher IBR/n values indicate a greater integrated deviation across the biomarker suite relative to the standardised control profile. Data are presented as mean ± SD ($n = 9$). IBR/n is interpreted as a descriptive integrative index, not as an independent inferential statistical test.

4.2. Coordinated alteration of superoxide anion, NO and PO responses

The simultaneous alteration of superoxide anion, NO, and PO levels indicates that PS-MPs affect both redox activity and immune effector functions of *A. euryacanthus* coelomocytes. The concentration-related increase in superoxide anion production provides evidence of enhanced pro-oxidant activity following PS-MP exposure. Because ROS generation is an integral component of cellular defense, moderate enhancement may represent an activated respiratory burst associated with particle recognition and cellular defense. Persistent elevation, however, can increase the oxidative burden of cells.

This interpretation is consistent with observations in *P. lividus*, where PS microbeads increased intracellular ROS and reactive nitrogen species (Murano et al., 2020). The present study further demonstrates that enhanced pro-oxidant activity can occur alongside changes in individual coelomocyte populations. NO exhibited a concentration-dependent but non-linear response, increasing at 0.5 mg/L but decreasing at 1 mg/L. This pattern suggests regulation of the cellular redox environment rather than a simple concentration-dependent response. Because superoxide anion and NO are closely interconnected redox mediators, their simultaneous alteration may influence oxidative and nitrosative signalling.

The reduction in PO activity provides an important functional complement to the increased pro-oxidant response. PO-associated reactions contribute to innate immune defense in invertebrates, and its suppression suggests that increased oxidative activity may occur alongside altered immune effector capacity. Similar reductions in PO and antioxidant activity were reported in *A. indicus* exposed to PS-MPs and EPS-MPs (Barua et al., 2021). Collectively, the observed changes suggest a potential sequence in which PS-MP exposure is associated with enhanced superoxide generation and altered NO production, followed by disturbance of redox homeostasis and immune effector activity. Modulation of antioxidant and detoxification systems, including SOD, CAT, and GST, may subsequently represent compensatory responses to the increased reactive-species burden.

4.3. Cell-specific ROS generation demonstrates differential sensitivity of coelomocytes

A major strength of the present study is the resolution of ROS responses according to coelomocyte morphotype. Flow cytometric DCFDA analysis demonstrated pronounced increases in oxidant-sensitive fluorescence, particularly in G1- and G2-gated coelomocytes, following PS-MP exposure. After 7 days, G1 and G3 populations exhibited concentration-related increases in DCF fluorescence, whereas after 14 days the response became more cell-type-specific. G2 cells displayed particularly high fluorescence at 1 mg/L, while G3 cells showed their maximum response at 0.5 mg/L.

The non-linear G3 response indicates that prolonged exposure does not necessarily produce a simple linear increase in cellular ROS with increasing external concentration. Cellular phenotype, metabolic status, and population redistribution may contribute to this variation. Similar concentration- and time-dependent responses have been reported in other marine organisms exposed to PS particles. Huang et al. (2021) demonstrated that environmentally relevant PS exposure in *Mytilus coruscus* produced oxidative and immunological disturbances accompanied by metabolic reorganisation, with some biochemical responses returning toward control levels following recovery.

The cell-specific ROS profiles therefore suggest differential sensitivity of coelomocyte populations to PS-MP-associated oxidative challenge. G1-gated blast-like cells appeared more responsive, whereas G3-gated petaloid cells showed comparatively lower inducibility despite higher basal ROS levels. The attenuation or non-linearity of responses after 14 days may reflect compensatory antioxidant regulation, cellular adaptation, or changes in population composition; however, these mechanisms remain to be experimentally verified. Similar alterations in coelomocyte protein profiles following PS-MP exposure have been reported in *P. lividus* (Murano et al., 2023), supporting the concept that microplastic-associated stress may not be uniformly distributed among immune-cell populations.

4.4. Time-resolved ROS imaging reveals sustained oxidative activity

Confocal and time-lapse imaging complemented the endpoint flow-cytometric measurements by demonstrating the temporal progression of intracellular DCF fluorescence. The progressive increase in fluorescence over the 240-s observation period indicates continued accumulation of oxidant-sensitive DCF within individual coelomocytes following PS-MP exposure. The cell-to-cell variability further demonstrates heterogeneity in oxidative responsiveness, consistent with the morphological and functional diversity of coelomocytes.

The combination of flow cytometry and time-resolved microscopy therefore provides complementary information on population-level and cellular-level oxidative responses. However, a control time-lapse series was not included in the present experiment; consequently, the temporal fluorescence progression should be interpreted as supportive evidence of the exposure-associated oxidative response rather than as an independent demonstration of treatment-specific fluorescence kinetics. This limitation should be considered when interpreting the time-resolved imaging results. A limitation of the present time-lapse analysis is that a parallel control time-lapse series was not included. Therefore, the observed temporal increase in fluorescence should be interpreted as supportive evidence of the oxidative response following PS-MP exposure rather than as a direct comparison of treatment-specific fluorescence kinetics. Future studies incorporating matched control and exposure time-lapse series would help further distinguish exposure-associated changes from baseline temporal variation in DCF fluorescence.

4.5. Alteration of antioxidant defense and detoxification responses

The coordinated alteration of SOD, CAT, and GST demonstrates reorganisation of the antioxidant and detoxification systems of *A. euryacanthus* coelomocytes. SOD activity decreased following PS-MP exposure, with strongest suppression at 0.5 mg/L and partial recovery at 1 mg/L. CAT exhibited a consistent reduction across exposure concentrations, whereas GST activity increased progressively with concentration and exposure duration.

The decrease in SOD and CAT together with enhanced GST activity indicates that PS-MP exposure affects different components of cellular defense in distinct ways. SOD and CAT constitute major enzymatic defenses against reactive oxygen species, whereas GST contributes to glutathione-dependent detoxification and cellular protection. The induction of GST may therefore represent recruitment of an additional protective pathway during sustained exposure.

Comparable responses have been documented in other marine species. Wang et al. (2020) demonstrated that PS-MP exposure altered antioxidant responses in *Mytilus coruscus*, with the magnitude and direction of individual enzyme responses depending on environmental conditions such as seawater pH. Wang et al. (2021) further reported that particle size, exposure route, and food availability influenced physiological and antioxidant responses to PS particles. Shiry et al. (2023) also reported altered antioxidant physiology, oxidative stress, and increased haemocyte abundance in *Astacus leptodactylus* following prolonged microplastic-associated exposure.

Thus, the antioxidant profile observed in *A. euryacanthus* provides an important biochemical dimension to the cellular responses and generates a recognisable oxidative-defense signature characterised by SOD and CAT suppression together with GST induction.

4.6. Comparison with PS-MP responses in other echinoderms

The present findings contribute to increasing evidence that echinoderms are responsive to microplastic contamination. Murano et al.

(2020) demonstrated uptake and tissue distribution of PS microbeads in *P. lividus*, together with increased immune-cell abundance and early oxidative or nitrosative responses. Murano et al. (2023) subsequently demonstrated concentration-dependent alterations in the sea urchin coelomocyte proteome following PS-MP exposure, providing molecular evidence for effects on immune-cell metabolism and cellular processes.

Similarly, recent studies on the tropical sea cucumber *Holothuria leucospilota* reported that plastic exposure can influence oxidative stress, immune status, metabolism, and tissue integrity (Maldeniya et al., 2024, 2025). Collectively, these studies support the present observation that microplastic exposure can produce integrated alterations in immune-cell homeostasis and redox regulation. The present study extends this evidence to a tropical benthic asteroid by combining coelomocyte abundance, flow-cytometric morphotyping, intracellular ROS measurements, imaging, and biochemical antioxidant biomarkers within a common experimental framework.

4.7. Integrated biomarker response and biomarker application for field assessment

IBR analysis provides a descriptive integrative representation of the cellular and biochemical responses observed in *A. euryacanthus*. Rather than representing an inferential statistical framework, the IBR integrates multiple biomarker responses into a unified profile of PS-MP-associated physiological disturbance. This is useful because no single biomarker captures the complete biological response. Increased coelomocyte abundance may indicate immune mobilisation, while increased superoxide anion and DCF fluorescence indicate enhanced oxidative activity; changes in SOD, CAT, and GST further reflect modulation of antioxidant and detoxification processes.

Recent applications have demonstrated the utility of integrated biomarker approaches in marine organisms. Zhong et al. (2024) used IBR to integrate oxidative, immune, metabolic, and physiological responses in *M. coruscus* exposed to PS and PLA microplastics. In the present study, IBR similarly provides a descriptive overview of the combined biomarker response and complements, rather than replaces, the individual statistical analyses.

The ecological relevance of these findings extends beyond biochemical perturbations because coelomocytes are directly involved in innate immune protection in sea stars. Persistent alterations in immune-cell composition, oxidative balance, and antioxidant capacity may influence the ability of individuals to respond to pathogens and other environmental challenges. Consequently, these cellular and biochemical responses may have implications for the physiological resilience of benthic sea stars exposed to coastal contaminants.

Importantly, the present study did not directly demonstrate internalization or intracellular localization of PS-MPs. The observed cellular responses should therefore be interpreted as associated with exposure to PS-MPs, rather than as evidence that the particles were demonstrably internalized by coelomocytes. In addition, the tested concentrations should be considered acute/high-dose exposure scenarios relative to reported field concentrations. Although these concentrations are useful for characterising cellular and biochemical responses, the magnitude and persistence of effects under chronic exposure to environmentally relevant, lower concentrations remain uncertain. Future studies using environmentally realistic concentrations and longer exposure periods, together with direct particle-localisation approaches, would help establish the ecological significance of these responses.

Overall, the present study establishes a biomarker framework comprising coelomocyte abundance, coelomocyte morphotype distribution, superoxide anion, PO, SOD, CAT, GST, intracellular ROS measurements, and descriptive IBR for evaluating PS-MP-associated stress in *A. euryacanthus*. Application of this framework to wild sea stars from contrasting coastal environments could provide a biological complement to conventional measurements of environmental microplastic contamination.

5. Conclusion

This study provides a comprehensive cellular and biochemical framework for evaluating PS-MP-associated stress in the tropical benthic sea star *A. euryacanthus*. By integrating coelomocyte profiling, flow cytometric analysis, time-resolved confocal imaging, and IBR, this study advances beyond single-endpoint assessments and provides a more resolved basis for evaluating microplastic-associated effects in echinoderms. Future research should focus on the field validation of the identified coelomocyte biomarkers in wild *A. euryacanthus* across contrasting coastal environments, alongside measurements of environmental microplastic burden. Particular emphasis should be placed on evaluating the consistency of coelomocyte abundance and morphotype distribution, prooxidant and antioxidant responses as biomarker signatures, with the IBR providing an integrated measure of organismal stress. Such field-based validation, complemented by seasonal and long-term observations, will help establish the applicability of this biomarker framework for the routine biomonitoring of PS-MP pollution in tropical coastal ecosystems, particularly along the Bay of Bengal. It should be noted that the PS-MP concentrations tested in the present study are relatively high compared with reported field levels, highlighting the need for chronic exposure studies using lower, environmentally relevant concentrations to determine whether similar cellular and biochemical responses occur under more environmentally realistic exposure conditions. Three complementary experimental directions are particularly important for advancing this study. First, chronic exposure experiments using lower, environmentally relevant PS-MP concentrations are needed to evaluate responses under exposure scenarios that more closely represent persistent contamination in coastal habitats. Second, transmission electron microscopy (TEM) of tissue sections should be employed to directly visualise and confirm microplastic internalisation and tissue-level localisation. Third, molecular validation of haematopoiesis- and apoptosis-related regulatory pathways should be performed to determine the cellular processes underlying alterations in coelomocyte populations. Collectively, these approaches will strengthen the ecological interpretation of the present findings and support the development of *A. euryacanthus* as a sentinel species for microplastic pollution assessments in tropical coastal ecosystems.

CRediT authorship contribution statement

Abhinandan Barua: Writing – review & editing, Software, Methodology, Formal analysis, Conceptualization, Data curation, Writing – original draft. **Nairit Panday:** Writing – review & editing, Software, Methodology, Formal analysis, Data curation. **Ritwik Guchait:** Writing – review & editing, Methodology, Formal analysis. **Pritam Sinha:** Validation, Software, Formal analysis. **Arunodaya Gautam:** Writing – review & editing, Writing – original draft, Visualization, Validation, Supervision, Software, Resources, Project administration, Methodology, Investigation, Funding acquisition, Formal analysis, Data curation, Conceptualization. **Indrani Chakraborty:** Writing – review & editing, Writing – original draft, Supervision, Resources, Project administration, Methodology, Investigation, Formal analysis, Data curation, Conceptualization.

Declaration of Generative AI and AI-assisted technologies in the writing process

During the preparation of this work, the authors used CHATGPT 5.6 to improve the language in the Results and Discussion sections. Following the use of this tool, the authors critically reviewed and, where necessary, revised the generated content and assumed full responsibility for the accuracy, integrity, and final content of the article.

Declaration of competing interest

The authors declare that they have no competing financial or personal interests that could have influenced the work reported in this article. This study was supported exclusively by public research funding, and no commercial or industrial entities were involved in the design, conduct, analysis, or reporting of the research.

Acknowledgements

The authors acknowledge Estuarine and Coastal Studies Foundation, Howrah, for primary funding and logistic supports. The authors further acknowledge Department of Life science & Bio-technology of Jadavpur University, the Centre for Research in Nanoscience and Nanotechnology of the University of Calcutta, Jogamaya Devi College, Kolkata and Department of Chemistry, Maulana Azad College, Kolkata for providing logistics and instrumentation facilities.

Data availability

Data will be made available on request.

References

Aebi, H., 1984. Catalase in vitro. Methods Enzymol. 105, 121–126. https://doi.org/10.1016/S0076-6879(84)05016-3.

Alam, M.J., Shammi, M., Tareq, S.M., 2023. Distribution of microplastics in shoreline water and sediment of the Ganges River Basin to Meghna Estuary in Bangladesh. Ecotoxicol. Environ. Saf. 266, 115537. https://doi.org/10.1016/j.ecoenv.2023.115537.

Ashida, M., Söderhäll, K., 1984. The prophenoloxidase activating system in crayfish. Comp. Biochem. Physiol. B 77, 21–26. https://doi.org/10.1016/0305-0491(84)90217-7.

Barua, A., Gautam, A., Mukherjee, S., Pal, K., Karmakar, P., Ray, M., Ray, S., 2021. Expanded polystyrene microplastic is more cytotoxic to seastar coelomocytes than its non-expanded counterpart: a comparative analysis. J. Hazard. Mater. Lett. 2, 100031. https://doi.org/10.1016/j.hazl.2021.100031.

Beliaeff, B., Burgeot, T., 2002. Integrated biomarker response: a useful tool for ecological risk assessment. Environ. Toxicol. Chem. 21, 1316–1322. https://doi.org/10.1002/etc.5620210629.

Chatterjee, N.H., Das, S., Choudhury, A., Ray, S., 2025. Microplastic toxicity in aquatic organisms across phylogeny. Aquat. Toxicol. 287, 107501. https://doi.org/10.1016/j.aquatox.2025.107501.

Coteur, G., Gillan, D., Joly, G., Pernet, P., Dubois, P., 2003. Field contamination of the starfish *Asterias rubens* by metals. Part 2: effects on cellular immunity. Environ. Toxicol. Chem. 22, 2145–2151. https://doi.org/10.1897/02-490.

EFSA Panel on Food Contact Materials, Enzymes and Processing Aids (CEP), 2020. Assessment of the impact of the IARC monograph vol. 121 on the safety of the substance styrene (FCM No 193) for its use in plastic food contact materials. EFSA J. 18, 6247. https://doi.org/10.2903/j.efsa.2020.6247.

El Hadri, H., Gigault, J., Maxit, B., Grassl, B., Reynaud, S., 2020. Nanoplastic from mechanically degraded primary and secondary microplastics for environmental assessments. NanoImpact 17, 100206. https://doi.org/10.1016/j.impact.2019.100206.

Green, L.C., Wagner, D.A., Glogowski, J., Skipper, P.L., Wishnok, J.S., Tannenbaum, S.R., 1982. Analysis of nitrate, nitrite, and [15N]nitrate in biological fluids. Anal. Biochem. 126, 131–138. https://doi.org/10.1016/0003-2697(82)90118-X.

Habig, W.H., Pabst, M.J., Jakoby, W.B., 1974. Glutathione S-transferases: the first enzymatic step in mercapturic acid formation. J. Biol. Chem. 249, 7130–7139. https://doi.org/10.1016/S0021-9258(19)42083-8.

Huang, W., Wang, X., Chen, D., Xu, E.G., Luo, X., Zeng, J., Huan, T., Li, L., Wang, Y., 2021. Toxicity mechanisms of polystyrene microplastics in marine mussels revealed by high-coverage quantitative metabolomics using chemical isotope labeling liquid chromatography mass spectrometry. J. Hazard. Mater. 417, 126003. https://doi.org/10.1016/j.jhazmat.2021.126003.

Kankanige, D., Babel, S., 2020. Smaller-sized micro-plastics (MPs) contamination in single-use PET-bottled water in Thailand. Sci. Total Environ. 717, 137232. https://doi.org/10.1016/j.scitotenv.2020.137232.

Kuthan, H., Haussmann, H.-J., Werringloer, J., 1986. A spectrophotometric assay for superoxide dismutase activities in crude tissue fractions. Biochem. J. 237, 175–180. https://doi.org/10.1042/bj2370175.

Lütken, C.F., 1871. Continued critical and descriptive contributions to the knowledge of starfish (asteroids). Sci. Rep. Dan. Nat. Hist. Soc. 1871, 227–304. https://www.biodiversitylibrary.org/page/35853627.

Maldeniya, M.U.S., Liu, Y., Ma, B., Yin, J., Wen, S., Yuan, L., Luo, P., 2025. Microplastic and nanoplastic exposure induced transcriptional and physiological alterations and triggered immune responses in the sea cucumber, *Holothuria leucospilota*. Environ. Pollut. 375, 126291. https://doi.org/10.1016/j.envpol.2025.126291.

Maldeniya, M.U.S., Ma, B., Liu, Y., Yin, J., Pan, W., Wen, S., Luo, P., 2024. Potential harmful impacts of micro- and nanoplastics on the health of a tropical sea cucumber, *Holothuria leucospilota*, evidenced by changes of gut microflora, histology, immune and oxidative indexes. Sci. Total Environ. 954, 176487. https://doi.org/10.1016/j.scitotenv.2024.176487.

Manna, S., Ray, A., Gautam, A., Mukherjee, S., Ray, M., Ray, S., 2022. A comparative account of coelomocyte of earthworm ecotypes with reference to its morphology, morphometry, density, phagocytosis, autofluorescence, and oxidative status. J. Morphol. 283, 956–972. https://doi.org/10.1002/jmor.21483.

Mazur, A.A., Chelomin, V.P., Zhuravel, E.V., Kukla, S.P., Slobodskova, V.V., Dovzhenko, N.V., 2021. Genotoxicity of polystyrene (PS) microspheres in short-term exposure to gametes of the sand dollar *Scaphechinus mirabilis* (Agassiz, 1864) (Echinodermata, Echinoidea). J. Mar. Sci. Eng. 9, 1088. https://doi.org/10.3390/jmse9101088.

Morroni, L., Rakaj, A., Grosso, L., Flori, G., Fianchini, A., Pellegrini, D., Regoli, F., 2023. Echinoderm larvae as bioindicators for the assessment of marine pollution: sea urchin and sea cucumber responsiveness and future perspectives. Environ. Pollut. 335, 122285. https://doi.org/10.1016/j.envpol.2023.122285.

Murano, C., Agnisola, C., Caramiello, D., Castellano, I., Casotti, R., Corsi, I., Palumbo, A., 2020. How sea urchins face microplastics: uptake, tissue distribution and immune system response. Environ. Pollut. 264, 114685. https://doi.org/10.1016/j.envpol.2020.114685.

Murano, C., Nonnis, S., Scalvini, F.G., Maffioli, E., Corsi, I., Tedeschi, G., Palumbo, A., 2023. Response to microplastic exposure: an exploration into the sea urchin immune cell proteome. Environ. Pollut. 320, 121062. https://doi.org/10.1016/j.envpol.2023.121062.

Pinsino, A., Della Torre, C., Sammarini, V., Bonaventura, R., Amato, E., Matranga, V., 2008. Sea urchin coelomocytes as a novel cellular biosensor of environmental stress: a field study in the Tremiti Island Marine Protected Area, Southern Adriatic Sea, Italy. Cell Biol. Toxicol. 24, 541–552. https://doi.org/10.1007/s10565-008-9055-0.

Pinsino, A., Thorndyke, M.C., Matranga, V., 2007. Coelomocytes and post-traumatic response in the common sea star *Asterias rubens*. Cell Stress Chaperones 12, 331–341. https://doi.org/10.1379/CSC-288.1.

Queiroz, V., Custódio, M.R., 2025. Diversity of coelomocytes in the class Echinoidea (Echinodermata): a comparative study based on morphological evidence. Comp. Immunol. Rep. 8, 200212. https://doi.org/10.1016/j.cirep.2025.200212.

Ragusa, A., Notarstefano, V., Svelato, A., Belloni, A., Gioacchini, G., Blondeel, C., Zucchelli, E., De Luca, C., D'Avino, S., Gulotta, A., Carnevali, O., Giorgini, E., 2022. Raman microspectroscopy detection and characterisation of microplastics in human breastmilk. Polymers 14, 2700. https://doi.org/10.3390/polym14132700.

Richardson, C.R., Burritt, D.J., Allan, B.J.M., Lamare, M.D., 2021. Microplastic ingestion induces asymmetry and oxidative stress in larvae of the sea urchin *Pseudechinus huttoni*. Mar. Pollut. Bull. 168, 112369. https://doi.org/10.1016/j.marpolbul.2021.112369.

Shirmohammadi, M., Kianersi, F., Shiry, N., Hekmatpour, F., 2025. Ecotoxicological assessment of microplastics and florfenicol on Acanthopagrus latus: mucus, humoral immune responses and DNA damage. Ecotoxicology 34, 1128–1143. https://doi.org/10.1007/s10646-025-02901-z.

Shiry, N., Darvishi, P., Gholamhossieni, A., Pastorino, P., Faggio, C., 2023. Exploring the combined interplays: effects of cypermethrin and microplastic exposure on the survival and antioxidant physiology of *Astacus leptodactylus*. J. Contam. Hydrol. 259, 104257. https://doi.org/10.1016/j.jconhyd.2023.104257.

Shiry, N., Shirmohammadi, M., Faggio, C., 2026. Fate and transport of microplastics in aquatic ecosystems. In: Nguyen, M.K., Pham, M.T., Wang, L.C. (Eds.), Plastic Pollution in Aquatic Systems: Challenges, Strategies, and Innovative Solutions for a Circular Economy. Elsevier, pp. 35–54. https://doi.org/10.1016/B978-0-443-45248-2.00018-3.

Smith, V.J., 2010. Immunology of invertebrates: cellular. eLS 1–13. https://doi.org/10.1002/9780470015902.a0000958.pub2.

Sun, H., Jiao, R., Wang, D., 2021. The difference of aggregation mechanism between microplastics and nanoplastics: role of Brownian motion and structural layer force. Environ. Pollut. 268, 115942. https://doi.org/10.1016/j.envpol.2020.115942.

Takahashi, K., Akaike, T., Sato, K., Mori, K., Maeda, H., 1993. Superoxide anion generation by Pacific oyster (Crassostrea gigas) hemocytes: identification by electron spin resonance spin trapping and chemiluminescence analysis. Comp. Biochem. Physiol. B 105, 32–41. https://doi.org/10.1016/0305-0491(93)90166-3.

Tang, J., Ni, X., Zhou, Z., Wang, L., Lin, S., 2018. Acute microplastic exposure raises stress response and suppresses detoxification and immune capacities in the scleractinian coral *Pocillopora damicornis*. Environ. Pollut. 243, 66–74. https://doi.org/10.1016/j.envpol.2018.08.040.

Teuten, E.L., Saquing, J.M., Knappe, D.R.U., Barlaz, M.A., Jonsson, S., Björn, A., Rowland, S.J., Thompson, R.C., Galloway, T.S., Yamashita, R., Ochi, D., Watanuki, Y., Moore, C., Pham Hung Viet, N., Tana, T.S., Prudente, M., Boonyatumanond, R., Zakaria, M.P., Akkhavong, K., Ogata, Y., Hirai, H., Iwasa, S., Mizukawa, K., Hagino, Y., Imamura, A., Saha, M., Takada, H., 2009. Transport and release of chemicals from plastics to the environment and to wildlife. Philos. Trans. R. Soc. B Biol. Sci. 364, 2027–2045. https://doi.org/10.1098/rstb.2008.0284.

Wahltinez, S.J., Kroll, K.J., Behringer, D.C., Arnold, J.E., Whitaker, B., Newton, A.L., Edmiston, K., Hewson, I., Stacy, N.I., 2023. Common sea star (*Asterias rubens*) coelomic fluid changes in response to short-term exposure to environmental stressors. Fishes 8, 51. https://doi.org/10.3390/fishes8010051.

Wang, S., Zhong, Z., Li, Z., Wang, X., Gu, H., Huang, W., Fang, J.K.-H., Shi, H., Hu, M., Wang, Y., 2021. Physiological effects of plastic particles on mussels are mediated by food presence. J. Hazard. Mater. 404, 124136. https://doi.org/10.1016/j.jhazmat.2020.124136.

Wang, X., Huang, W., Wei, S., Shang, Y., Gu, H., Wu, F., Lan, Z., Hu, M., Shi, H., Wang, Y., 2020. Microplastics impair digestive performance but show little effects on antioxidant activity in mussels under low pH conditions. Environ. Pollut. 258, 113691. https://doi.org/10.1016/j.envpol.2019.113691.

Wesch, C., Bredimus, K., Paulus, M., Klein, R., 2016. Monitoring ingestion of microplastics by marine biota. Environ. Pollut. 218, 1200–1208. https://doi.org/10.1016/j.envpol.2016.08.055.

Zhong, Z., Shang, W., Yang, P., Wang, S., Chen, L., Chen, Z., Li, L., Khalil, M.F., Hu, M., Xu, X., Wang, Y., 2024. Bio-based microplastic polylactic acid exerts the similar toxic effects to traditional petroleum-based microplastic polystyrene in mussels. Sci. Total Environ. 946, 174386. https://doi.org/10.1016/j.scitotenv.2024.174386.